University of Nebraska - Lincoln
DigitalCommons@University of Nebraska - Lincoln

Xiao Cheng Zeng Publications | Published Research - Department of Chemistry

7-22-2002

Heterogeneous nucleation on mesoscopic wettable particles: A hybrid thermodynamic/density-functional theory

T.V. Bykov
University of Nebraska-Lincoln

Xiao Cheng Zeng
University of Nebraska-Lincoln, xzeng1@unl.edu

Follow this and additional works at: https://digitalcommons.unl.edu/chemzeng

 Part of the Chemistry Commons

Bykov, T.V. and Zeng, Xiao Cheng, "Heterogeneous nucleation on mesoscopic wettable particles: A hybrid thermodynamic/density-functional theory" (2002). *Xiao Cheng Zeng Publications*. 41.
https://digitalcommons.unl.edu/chemzeng/41

This Article is brought to you for free and open access by the Published Research - Department of Chemistry at DigitalCommons@University of Nebraska - Lincoln. It has been accepted for inclusion in Xiao Cheng Zeng Publications by an authorized administrator of DigitalCommons@University of Nebraska - Lincoln.

Heterogeneous nucleation on mesoscopic wettable particles: A hybrid thermodynamic/density-functional theory

T. V. Bykov and X. C. Zeng[a)]
Department of Chemistry, University of Nebraska—Lincoln, Lincoln, Nebraska 68588

(Received 15 February 2002; accepted 23 April 2002)

A hybrid thermodynamic and density-functional theory for heterogeneous nucleation on mesoscopic wettable particles is developed. The nonlocal density-functional theory (DFT) is on basis of the weighted-density approximation (WDA) of Tarazona. The model system consists of a Lennard-Jones (LJ) fluid and a 9–3 LJ wall for the solid particle. Effects of the droplet curvature and compressibility are accounted for in the theory. A by-product of this work is the calculation of the Tolman length using the WDA-DFT (Appendix A). Important characteristics of the heterogeneous nucleation, including the chemical potential of the liquid condensate, the free energy of droplet formation, and the barrier height to nucleation, are obtained. © *2002 American Institute of Physics.* [DOI: 10.1063/1.1485733]

I. INTRODUCTION

Heterogeneous nucleation is the most common mechanism in initiating a first-order phase transition. For example, from a metastable supersaturated vapor to the bulk liquid, the nucleation process often proceeds with the formation of a liquid-like film on the surface of foreign particles. Many kinds of particles can act as heterogeneous-nucleation centers. These include ions, droplets of acid, solutable or unsolutable sols, and dust particles. It is known that thermodynamic properties of the liquid film formed on the surface of a particle depend strongly on the nature of the surface force. A general feature for heterogeneous nucleation is the existence of a threshold supersaturation beyond which the so-called barrierless nucleation can take place. In comparison, the homogeneous nucleation which occurs only in an impurity-free environment, is much less common in nature. In fact, the homogeneous nucleation always requires a higher value of supersaturation than that for heterogeneous nucleation. This was first recognized by Volmer[1] in 1939. Since then, studies of heterogeneous nucleation have received considerable attention. Recent reviews on this subject can be found in Refs. 2–4.

In this paper we consider the heterogeneous nucleation on mesoscopic spherical particles. Droplet formation on the particles can be developed in two ways, depending on the wettability of the liquid on the surface of the particle. The first possible way is the formation of a liquid film on the entire surface of the particle (complete wetting). The film then grows into a large liquid droplet with the foreign particle at the center. The second way is via forming microlenses of liquid on the surface of the particle with a nonzero contact angle. These separate microlenses then grow in size, collapse into a thick film which covers the entire surface of the particle, and then develop into a large liquid droplet. In this study, we consider only the first possibility. A sufficient condition for this possibility is that the liquid condensate will wet the surface of the particle completely as the radius approaches infinity (or the coefficient of spreading of the condensate is positive in the planar limit[2]).

As mentioned above, the thermodynamic properties of the liquid condensate on the mesoscopic particles strongly depend on the nature of the surface force. In the classical theory of heterogeneous nucleation,[2,4,5] several empirical parameters were introduced to describe the surface forces. These parameters are generally taken either from experiments or from other microscopic theories or molecular simulations, for example, the molecular theory of capillarity and the density-functional theory, or molecular dynamics and Monte Carlo simulations. Molecular simulations have been used extensively to explore various wetting phenomena on a planar solid surface,[6–9] and have yielded important results such as the dependence of wetting temperature and the surface critical temperature on the surface force, as well as the density profiles of the liquid film near the solid surface. Density-functional theory (DFT) has also been employed by many workers to study behavior of a fluid near a solid surface.[10–14] In most studies, the so-called weighted density approximation (WDA) developed by Tarazona[10,11] is adopted. The WDA has been shown to be very accurate for describing highly nonuniform solid–liquid interfacial systems.[8,9,14] Both DFT and molecular simulations have their own advantages and shortcomings. In molecular simulations, the number of molecules in the simulation cell is finite (typically, a few thousand), whereas a typical mesoscopic size of droplet possesses at least millions of molecules. Although DFT is free from such size limitation, it requires certain approximation in the correlation function and free-energy functional, which renders the calculation less accurate. Here, we use the DFT because we are interested in the formation of liquid droplets on mesoscopic particles. Moreover, the DFT has been used in many previous studies of homogeneous nucleation.[15]

As discussed above, a planar surface can be considered as the limiting case for a mesoscopic particle when its diameter approaches infinity. For the planar surface, the complete wetting may occur when the nucleating vapor is undersatu-

a)Electronic mail: xzeng1@unl.edu

 © 2002 American Institute of Physics

Downloaded 18 Apr 2007 to 129.93.16.206. Redistribution subject to AIP license or copyright, see http://jcp.aip.org/jcp/copyright.jsp

rated. Towards the complete wetting, the disjoining potential changes monotonically as a function of the thickness of the liquid film (see, for example, Fig. 1 in Ref. 14), while it is nonmonotonic for the incomplete wetting. Thus far, most DFT studies on the heterogeneous nucleation focus mainly upon systems involving partially wettable particles,[16,17] namely, the second possible way of heterogeneous nucleation described above. In that case, the line tension of the three-phase interface on the solid surface must be considered. The solid surface can be either planar[18] or curved.[19,20] DFT with a local gradient expansion was the basis for all these studies. It is well known that the local density approximation (LDA) cannot qualitatively describe the structure of the density profile near the solid surface. Thus, we will use the nonlocal WDA-DFT.[10,11] We will present a hybrid approach by combining the DFT with a classical nucleation theory.[2,4] The latter[2,4] yields general relations among thermodynamical and kinetic properties of the system, while the DFT provides important properties of the liquid droplet, such as the dependence of the chemical potential of the liquid droplet on the droplet size. Outcomes of the hybrid theory include the threshold value of the chemical potential (or the threshold value of the supersaturation) for barrierless nucleation, the height of the activation barrier to nucleation, the half-width of the barrier, as well as the position of the minimum and maximum on the curve of free energy of droplet formation versus the droplet size.

This paper is organized as a follows: In Sec. II several main aspects of the thermodynamics of heterogeneous nucleation are discussed. In Sec. III the DFT with the WDA of Tarazona is briefly discussed and the application to a wetting liquid film on the planar solid surface is reviewed. Characteristics of the chemical potential of the liquid condensate are described and chemical potential of the liquid condensate as a function of molecular number in the liquid film is given in Sec. IV. Key properties of heterogeneous nucleation, such as the free energy of droplet formation and the barrier height to nucleation, are presented in Sec. V. Final conclusions are given in Sec. VI. In Appendix A, we present generalized Blokhuis-Bedeaux formulas for the surface tension and the Tolman length by accounting for the effect of the nonlocal WDA.

II. THERMODYNAMICS OF HETEROGENEOUS NUCLEATION

Several main thermodynamic equations such as the Laplace equation and Gibbs–Duhem equation form the basis for the description of any droplet-like object in the classical nucleation theory.[2] In this section we formulate generalized version of these equations for the description of heterogeneous nucleation on mesoscopic wettable particles.

The system considered here is an open system which consists of a mesoscopic wettable solid particle and a metastable vapor at a fixed temperature and volume. Upon condensation, a liquid film with a uniform thickness will form on the surface of particle (complete wetting). Assuming the system has spherical symmetry, the density profile of the system is given by $\rho(r)$, where r is the distance from the center of the solid particle. Hereafter, we refer the metastable vapor as phase 1, the liquid film as phase 2, and the solid particle as phase 3. In describing the thermodynamics of this nonuniform system, we use the Gibbs method of dividing surfaces to replace $\rho(r)$ by a step-like density profile, similar to the sharp-kink model introduced by Getta and Dietrich.[18] This new density profile consists of the solid particle with density ρ_3, the liquid film with density ρ_2 which equals the bulk density of liquid at the current supersaturation, and the vapor with density of ρ_1. The solid particle has a radius $\tilde{R}_n$. We use $\tilde{R}_n$ to represent its physical radius and R_n for the radius of the solid–liquid dividing surface. R_n may differ from $\tilde{R}_n$ by few molecular diameter, depending on the thickness of the solid–liquid interface. Following Ref. 18, we set zero density between $\tilde{R}_n$ and R_n. The radius of the liquid–vapor dividing surface is denoted by R. Thus, the thickness of the liquid film is given by $h=R-R_n$ (see Fig. 1). Finally, L denotes the outmost radius of the entire system. L can be chosen in such a way that beyond L the physical density of vapor is nearly uniform (i.e., ρ_1).

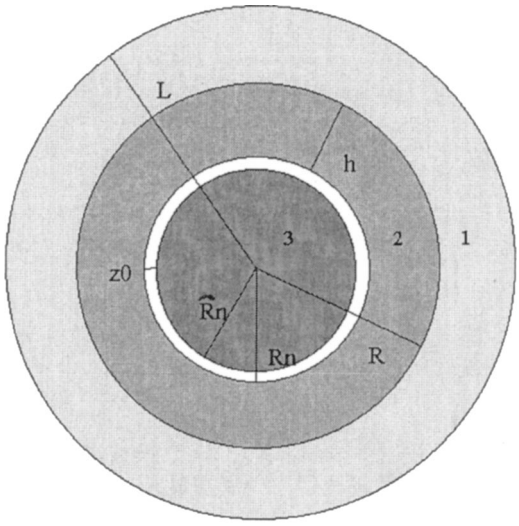

FIG. 1. A schematic plot of a liquid droplet forming on a mesoscopic wettable solid particle.

The supersaturation of the vapor is characterized by the chemical potential μ. At the fixed temperature, the vapor density ρ_1 is determined solely by μ, and so is the density of the bulk liquid ρ_2. For the open system, the grand thermodynamic potential is given by

$$\Omega = -p_2\frac{4\pi}{3}(R^3-R_n^3)-p_1\frac{4\pi}{3}(L^3-R^3) + 4\pi R_n^2\sigma_{32}(R_n)+4\pi R^2\sigma_{21}(R)+\tilde{\Omega}(h), \quad (1)$$

where p_2 is the normal pressure of the uniform liquid film (with the density ρ_2), p_1 is the pressure of the vapor (with the density ρ_1), $\sigma_{32}(R_n)$ is the surface tension of the solid–liquid interface, which depends on the curvature and the choice of the dividing surface R_n, and $\sigma_{21}(R)$ is the surface tension of the liquid–vapor interface, which also depends on the curvature and choice of the dividing surface R. Both $\sigma_{32}(R_n)$ and $\sigma_{21}(R)$ are defined such that they are independent of the thickness of the liquid film. In reality, this would

Downloaded 18 Apr 2007 to 129.93.16.206. Redistribution subject to AIP license or copyright, see http://jcp.aip.org/jcp/copyright.jsp

be true only if the film is thick so that the physical density of the film is nearly ρ_2. Equation (1) does not include the thermodynamic potential of the solid particle since it stays constant for all changes in the system.

The last term in Eq. (1), $\tilde{\Omega}(h)$, is a function of the thickness of liquid film h. It approaches zero as h goes to infinity. Assuming the spherical symmetry $\tilde{\Omega}(h)$ can be written as the integral from some volume density $\tilde{\omega}(r)$

$$\tilde{\Omega}(h)=4\pi\int_R^L r^2\tilde{\omega}(r)dr=4\pi\int_{R_n+h}^L r^2\tilde{\omega}(r)dr, \tag{2}$$

where the integration is taken from R to L, due to the removal of the bulk liquid from R to L, which creates the liquid film with a finite thickness. Thus, Eq. (1) can be rewritten as

$$\Omega+\frac{4\pi}{3}L^3p_1=-\frac{4\pi}{3}R^3(p_2-p_1)+\frac{4\pi}{3}R_n^3p_2 +4\pi R_n^2\sigma_{32}(R_n)+4\pi R^2\sigma_{21}(R) +4\pi\int_R^L r^2\tilde{\omega}(r)dr. \tag{3}$$

Taking a partial derivative over R on Eq. (3) under the condition of fixed μ and R_n, and noting that Ω, p_1, p_2, and $\sigma_{32}(R_n)$ do not depend on R, we obtain

$$0=-4\pi R^2(p_2-p_1)+8\pi R\sigma_{21}(R)+4\pi R^2\frac{\partial\sigma_{21}}{\partial R} +4\pi\frac{\partial}{\partial R}\int_R^L r^2\tilde{\omega}(r)dr, \tag{4}$$

or

$$p_2-p_1=\frac{2\sigma_{21}(R)}{R}+\frac{\partial\sigma_{21}}{\partial R}(R)-\tilde{\omega}(R_n+h). \tag{5}$$

Equation (5) can be considered as the generalized Laplace equation in the case of heterogeneous nucleation.

The second important thermodynamic equation is the generalized Gibbs–Duhem equation, which can be derived by taking the differential of Ω [Eq. (1)], under the condition of fixed temperature and total volume of the system

$$d\Omega=-4\pi p_2(R^2dR-R_n^2dR_n)-V_2\,dp_2+4\pi p_1R^2\,dR -V_1\,dp_1+8\pi R_n\sigma_{32}\,dR_n+4\pi R_n^2\,d\sigma_{32} +8\pi R\sigma_{21}\,dR+4\pi R^2\,d\sigma_{21}-4\pi R^2\tilde{\omega}(R)dR, \tag{6}$$

where V_1 and V_2 are the volume of the vapor and the liquid, respectively. On the other hand, we have

$$d\Omega=-N\,d\mu=-(N_{32}+N_2+N_{21}+N_1)d\mu, \tag{7}$$

where N is the total number of molecules (excluding that of the solid particle) in the system, which is the sum of the molecules in the liquid film N_2, vapor N_1, and two interfacial regions N_{32} and N_{21}. Combining Eq. (6) with Eq. (7) and noting that $dR_n=0$ (for fixed solid–particle size), $V_2\,dp_2=N_2\,d\mu$ (or $dp_2=\rho_2\,d\mu$) and $V_1\,dp_1=N_1\,d\mu$ (or $dp_1=\rho_1\,d\mu$), we obtain

$$-(p_2-p_1)4\pi R^2dR+4\pi R_n^2d\sigma_{32}+4\pi R^2d\sigma_{21}+8\pi R\sigma_{21}dR -4\pi R^2\tilde{\omega}(R_n+h)dh+N_{32}d\mu+N_{21}d\mu=0. \tag{8}$$

Substituting the generalized Laplace equation (5) into Eq. (8) results in the generalized Gibbs–Duhem equation

$$-4\pi R^2\frac{\partial\sigma_{21}}{\partial R}dR+4\pi R^2\,d\sigma_{21}+4\pi R_n^2\,d\sigma_{32}+N_{32}\,d\mu +N_{21}\,d\mu=0. \tag{9}$$

Equation (9) can be further separated into two equations

$$d\sigma_{32}=-\Gamma_{32}\,d\mu, \tag{10}$$

and

$$d\sigma_{21}-\frac{\partial\sigma_{21}}{\partial R}dR=-\Gamma_{21}\,d\mu, \tag{11}$$

by defining two adsorptions, Γ_{32} and Γ_{21}. $\Gamma_{32}=N_{32}/4\pi R_n^2$ is the adsorption of the liquid on the surface of the solid particle, and $\Gamma_{21}=N_{21}/4\pi R^2$ is the adsorption at the liquid–vapor interface.

The generalized Laplace equation (5) and generalized Gibbs–Duhem equations (10) and (11) are key thermodynamic equations for the study of heterogeneous nucleation. We note that in our consideration σ_{32} and σ_{21} in these equations depend only on the curvature of the droplet, but not on the thickness of the liquid film. Only $\tilde{\omega}(R_n+h)$ in Eq. (5) depends on the thickness h. The physical significance of the free-energy density $\tilde{\omega}(R_n+h)$ can be better illustrated from the limiting case of the liquid film (with thickness h) near a planar solid surface. In this limit the radial variable r can be replaced by $z=r-\tilde{R}_n$, where the z axis is perpendicular to the solid surface with the origin at this surface. Thus, $\tilde{\omega}(r)$ becomes $\tilde{\omega}(z)=\lim_{\tilde{R}_n\to\infty}\tilde{\omega}(r)$. In fact, we will restrict our attention to that type of particles for which the solid–liquid interaction potential depends only on the distance from the particle surface. For these particles, the replacement r by z is always valid.

Note that in the limiting case of planar liquid–vapor interface σ_{21} is independent of the curvature, namely, $\partial\sigma_{21}/\partial R|_{R\to\infty}=0$. Let $z_0=|\tilde{R}_n-R_n|$. Equations (5), (10), and (11) then become

$$p_2-p_1=-\tilde{\omega}(z_0+h), \tag{12}$$

$$d\sigma_{32}=-\Gamma_{32}\,d\mu, \tag{13}$$

and

$$d\sigma_{21}=-\Gamma_{21}\,d\mu, \tag{14}$$

respectively. Here, the bulk vapor pressure p_1 is also the normal component of pressure tensor at the interface and p_2 is the pressure of the bulk uniform liquid at the same μ. This means that p_1-p_2 is just the Derjaguin's disjoining pressure $\Pi(h)$[21] for the planar liquid film; thus, $\tilde{\omega}(z_0+h)=\Pi(h)$ according to Eq. (12). $\Pi(h)$ can be considered as a sum of several components:[21] some due to the overlapping of the interfacial layers of the thin liquid film while others due to the interactions between the solid surface and the liquid film. The h dependence of Π is the key characteristic of the liquid

Downloaded 18 Apr 2007 to 129.93.16.206. Redistribution subject to AIP license or copyright, see http://jcp.aip.org/jcp/copyright.jsp

film needed to develop theory of heterogeneous nucleation on solid surface. This dependence cannot be given from the classical nucleation theory.[2] DFT, on the other hand, can yield $\Pi(h)$, and numerical results will be given in the next section.

III. PROPERTIES OF THE LIQUID FILM NEAR PLANAR SOLID SURFACE: DFT, MODEL SYSTEM, AND THICKNESS DEPENDENCE

Let us first briefly summarize several main aspects of the WDA-DFT.[10,11] Let $w(\mathbf{r}_1,\mathbf{r}_2)=w(r_{12})$ represent the pairwise interaction molecular potential for the simple nonpolar molecules. In this case the free-energy functional of nonuniform system near planar solid surface (with the random-phase approximation) is given by[12–14]

$$F[\rho]=\int d\mathbf{r}\, f_{id}(\rho(z))+\int d\mathbf{r}\,\rho(z)\Delta\psi_{hs}(\overline{\rho}(z)) + \frac{1}{2}\int\int d\mathbf{r}_1\, d\mathbf{r}_2\, w_p(r_{12})\rho(z_1)\rho(z_2), \tag{15}$$

where z is the distance from the solid surface, $w_p(r_{12})$ is the small attractive part of interaction potential, and $f_{id}(\rho)$ is the free-energy density of the ideal gas. $\Delta\psi_{hs}(\overline{\rho})$ is the excess free-energy density, and it can be calculated accurately via the Carnahan–Starling[22] formula $\Delta\psi_{hs}(\rho)=k_BT\eta(4-3\eta)/(1-\eta)^2$, where k_B is the Boltzmann constant, T is the temperature, and $\eta=\pi\rho d^3/6$ (d is the hard-sphere diameter and ρ is the density). In Eq. (15), $\Delta\psi_{hs}(\overline{\rho})$ is a function of the weighted density $\overline{\rho}(z)$. The latter can be determined by averaging the true local density $\rho(z)$ over certain local volume. Following Tarazona,[10,11] we have

$$\overline{\rho}(z_1)=\int d\mathbf{r}_2\,\rho(z_2)\omega(r_{12},\overline{\rho}(z_1)), \tag{16}$$

where the weighting function ω is chosen in the same way as in Refs. 10 and 11.

In the grand canonical ensemble, the grand thermodynamic potential is given by

$$\Omega[\rho]=F[\rho]+\int d\mathbf{r}_1\,\rho(z_1)V_{ext}(z_1)-\mu\int d\mathbf{r}_1\,\rho(z_1), \tag{17}$$

where $V_{ext}(z_1)$ is the external potential (here, due to the solid surface). The equilibrium density profile is determined from the variational principle $\delta\Omega[\rho]/\delta\rho=0$, which gives

$$\rho(z_1)=\exp\left\{-\frac{1}{k_BT}\left[\int d\mathbf{r}_2\,\rho(z_2)\Delta\psi'_{hs}(\overline{\rho}(z_2))\times\frac{\omega(r_{12},\overline{\rho}(z_2))}{1-\overline{\rho}_1(z_2)-2\overline{\rho}_2(z_2)\overline{\rho}(z_2)}+\Delta\psi_{hs}(\overline{\rho}(z_1)) + \int d\mathbf{r}_2\, w_p(r_{12})\rho(z_2)+V_{ext}(z_1)-\mu\right]\right\}, \tag{18}$$

where $\overline{\rho_1}$ and $\overline{\rho_2}$ are defined in Refs. 10 and 11. The density profile $\rho(z)$ of the liquid film near a solid surface can be determined by solving the Eq. (18). To this end, we used an iteration method suggested by Tarazona.[10]

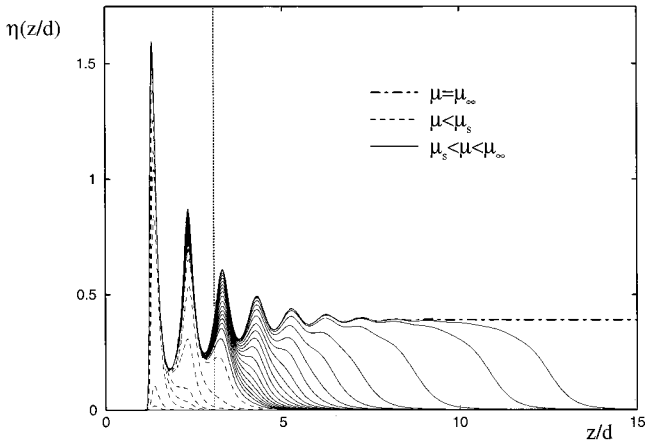

FIG. 2. The scaled density profile $\eta(z/d)=\rho(z/d)\pi d^3/6$ of LJ fluid films near an LJ 9–3 smooth planar wall located at $z=0$, for various given chemical potential μ at $T^*=k_BT/\epsilon_{\mathrm{LJ}}=0.9$. The vertical dotted line represents the position z_0/d.

The model system is chosen to be the Lennard-Jones (LJ) fluid near a 9–3 LJ smooth solid surface. In the framework of Weeks–Chandler–Anderson[23] perturbation scheme, we have

$$w_p(r_{12})=\begin{cases}-\epsilon_{\mathrm{LJ}}, & r_{12}<2^{1/6}\sigma,\\ 4\epsilon_{\mathrm{LJ}}[(\sigma/r_{12})^{12}-(\sigma/r_{12})^6], & r_{12}>2^{1/6}\sigma,\end{cases} \tag{19}$$

where ϵ_{LJ} and σ are the LJ parameters. The diameter of hard spheres (reference system) is related to σ, i.e., $d=(a_1T+a_4)/(a_2T+a_3)\sigma$, where the constants a_1, a_2, a_3, and a_4 are given in Ref. 24. The solid-surface potential[18] is given by

$$V_{ext}(z)=-\rho_3\left(\frac{u_3}{z^3}+\frac{u_9}{z^9}\right), \tag{20}$$

where $\rho_3=12/d^3$ is the density of the solid surface and coefficients u_3 and u_9 can be found as a result of summation for pairwise liquid–wall interactions over lattice structure of the wall. Following Getta and Dietrich[18] we use $u_3=2.348\epsilon_{\mathrm{LJ}}\sigma^6$ and $u_9=-5.326\epsilon_{\mathrm{LJ}}\sigma$.[12] For the numerical calculation, $V_{ext}(z)$ is set to be infinity for $z<0.84d$. The two reduced temperatures considered here are $T^*=k_BT/\epsilon_{\mathrm{LJ}}=0.7$ and 0.9; both are above the wetting temperature of the system as well as the surface critical temperature.

Using the iteration procedure, we have calculated $\rho(z)$ for several given chemical potential μ. The density profiles are shown in Fig. 2, which all exhibit the well-known oscillatory behavior near the solid surface. For $\mu=\mu_\infty$, the thickness h becomes infinity. Note that μ_∞ can be determined from the condition $p_1=p_2$. In the DFT, the bulk pressure is written as

$$p=p_h(\rho)-\tfrac{1}{2}\Psi\rho^2, \tag{21}$$

Downloaded 18 Apr 2007 to 129.93.16.206. Redistribution subject to AIP license or copyright, see http://jcp.aip.org/jcp/copyright.jsp

where $p_h(\rho)$ the pressure of the hard spheres[22] and $\Psi = -\int d\mathbf{r}\, w_p(r)$. For $\mu < \mu_\infty$, the liquid film has a finite thickness h, and p_1 and p_2 differs by Π, that is, the disjoining pressure.

Given the density profiles of the liquid films, we are ready to determine the thickness of the liquid film (h). For a planar liquid film near the solid surface, Eq. (1) can be written as

$$\overline{\Omega} = -p_2 h - p_1(\tilde{L} - h - z_0) + \sigma_{32} + \sigma_{21} + \tilde{\Omega}(h)/A, \quad (22)$$

where A is the surface area, $\overline{\Omega} = \Omega/A$, $\tilde{L}$ denotes the outmost boundary of the system, and z_0 is the distance between the solid–liquid dividing surface and the solid surface. The last term in Eq. (22) is

$$\begin{aligned}\tilde{\Omega}(h)/A &= \frac{4\pi}{A}\int_{R_n+h}^{L} r^2 \tilde{\omega}(r)dr \\ &= \frac{4\pi}{A}\int_{z_0+h}^{\tilde{L}} (R_n - z_0 + z)^2 \tilde{\omega}(z)dz \\ &= \frac{4\pi R_n^2}{A}\int_{z_0+h}^{\tilde{L}} (1 + (z-z_0)/R_n)^2 \tilde{\omega}(z)dz \\ &\to \int_{z_0+h}^{\tilde{L}} \tilde{\omega}(z)dz|_{R_n\to\infty} = \int_h^{\tilde{L}-z_0} \Pi(\tilde{h})d\tilde{h}. \quad (23)\end{aligned}$$

Using $p_1 - p_2 = \Pi(h)$ and Eq. (23), we rewrite Eq. (22) as

$$\overline{\Omega} + p_1(\tilde{L} - z_0) = \Pi(h)h + \sigma_{32} + \sigma_{21} + \int_h^{\tilde{L}-z_0} \Pi(\tilde{h})d\tilde{h}. \quad (24)$$

Although the left-hand side of Eq. (24) can be determined from the DFT, σ_{32}, σ_{21}, and h on the right-hand side are strongly dependent on the choice of the dividing surface.

For the liquid–vapor interface, we have chosen the equimolar dividing surface as the dividing surface so that $\Gamma_{21} = 0$. Thus, according to Eq. (14), σ_{21} will have a constant value regardless of μ, and this value is equal to the surface tension of the liquid–vapor interface $\sigma_{21}^{\infty} = \overline{\Omega}_\infty + p_{1\infty}\tilde{L}$ in the absence of the solid surface. For the solid–liquid interface, we have chosen the position of the dividing surface such that Γ_{32} is a constant. However, unlike Γ_{21}, Γ_{32} cannot be zero because there is always some liquid or vapor (even when $h = 0$) adsorbed on the solid surface. To determine Γ_{32} and z_0, we have used two limiting cases of h, one for h approaching infinity and the other for h approaching zero. The first case occurs when $\mu = \mu_\infty$ (see Fig. 2). The number of particles per unit surface area is given by

$$\int_0^{\tilde{L}} \rho(z)dz|_{\mu=\mu_\infty} = \Gamma_{32} + \rho_{2\infty}(\tilde{L} - z_0), \quad (25)$$

where $\rho_{2\infty}$ is the bulk density of the liquid at $\mu = \mu_\infty$. The second limiting case occurs when $\mu = \mu_s$, the chemical potential at liquid spinodal. The value of μ_s can be calculated from the DFT. For $\mu < \mu_s$ the bulk liquid phase does not exist, and thus ρ_2, p_2, and $\Pi(h)$ are not defined. This means one has to set the thickness $h = 0$. In this case the number of particles per unit surface area is given by

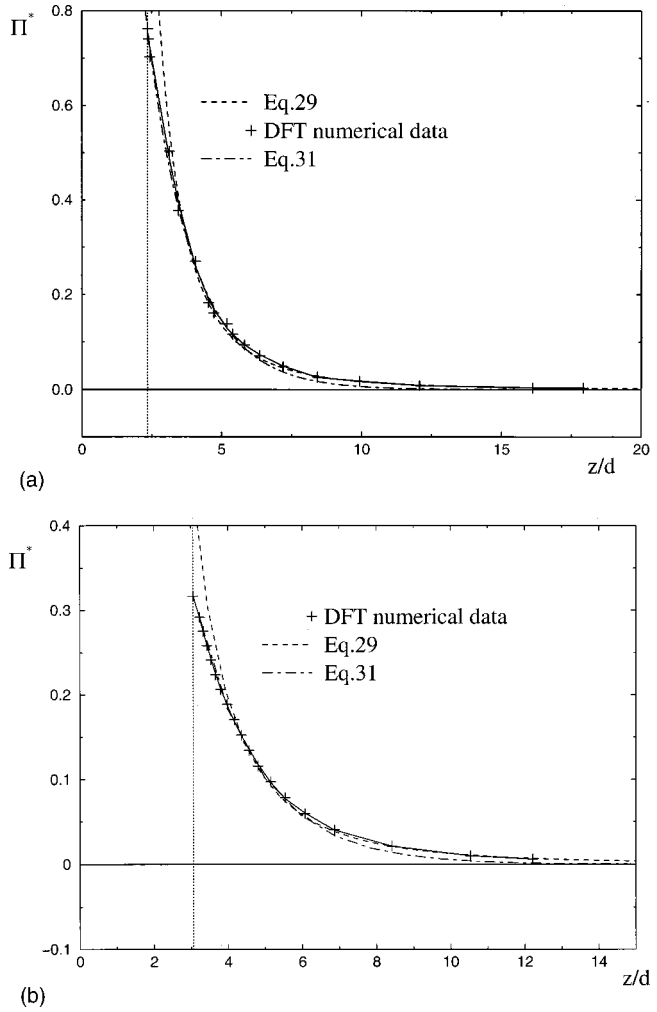

FIG. 3. The scaled disjoining pressure $\Pi^* = \Pi\pi d^3/6k_BT$ of the liquid film. The vertical dotted line represents the position z_0/d. (a) $T^* = 0.7$, $z_0 = 2.35d$, $B^* = \pi B/6k_BT = 16.9$, and $l = 1.6d$; (b) $T^* = 0.9$, $z_0 = 3.06d$, $B^* = \pi B/6k_BT = 12.5$, and $l = 1.7d$.

$$\int_0^{\tilde{L}} \rho(z)dz|_{\mu=\mu_s} = \Gamma_{32} + \rho_1|_{\mu=\mu_s}(\tilde{L} - z_0). \quad (26)$$

The left-hand side of both Eqs. (25) and (26) can be evaluated using the DFT. Thus, the two unknowns Γ_{32} and z_0 can be determined by solving the coupled Eqs. (25) and (26). Once Γ_{32} and z_0 are known, we can define the thickness of the film h for a given $\mu(\mu_s < \mu < \mu_\infty)$, that is,

$$h = \frac{\int_0^{\tilde{L}} \rho(z)dz - \Gamma_{32} - \rho_1(\tilde{L} - z_0)}{\rho_2 - \rho_1}. \quad (27)$$

With h defined, we turn to the main objective of this section, the thickness dependence of σ_{32} and Π. Integrating Eq. (13) with Γ_{32} fixed, we obtain

$$\sigma_{32} = \sigma_{32}^{\infty} - \Gamma_{32}(\mu - \mu_\infty), \quad (28)$$

where $\sigma_{32}^{\infty} = \overline{\Omega} + p_{2\infty}(\tilde{L} - z_0)$ is the solid–liquid surface tension when $h \to \infty$.

The dependence of Π on h for a given μ (between μ_s and μ_∞) is shown in Fig. 3. Indeed, $\Pi(h)$ is an essential input in the heterogeneous nucleation theory. In the classical

Downloaded 18 Apr 2007 to 129.93.16.206. Redistribution subject to AIP license or copyright, see http://jcp.aip.org/jcp/copyright.jsp

heterogeneous nucleation theory,[2] two commonly used approximations to $\Pi(h)$ are the power-law approximation and the exponential approximation. The former is for relatively thick liquid films, while the latter is for the thin structural films.[2] In the case of nonpolar LJ fluid, the power-law approximation to $\Pi(h)$ is given by

$$\Pi(h)\approx\frac{B}{(z_0+h)^3}, \tag{29}$$

where B is the Hamaker constant. However, the classical nucleation theory does not give this constant. In Ref. 18, a formula is given to estimate B based on the sharp-kink approximation to the density profile. According to this formula and in our notation, B is given by

$$B=(\rho_{2\infty}-\rho_{1\infty})(\rho_3 u_3-\rho_{2\infty}t_3), \tag{30}$$

where the subscript ∞ refers to $\mu=\mu_\infty$, and $t_3=-2\Psi/3\pi\sigma^3=64\sqrt{2}/27\sigma^6\epsilon_{\mathrm{LJ}}$ [using Eq. (19)]. To compare our result of $\Pi(h)$ to that of the power-law approximation, we set B as an independent parameter to fit the calculated $\Pi(h)$. The fitting shows that B is about 10% larger than that calculated from Eq. (30), indicating that Eq. (30) gives quite a good estimation of B. We conclude that the power-law approximation is in good agreement with the DFT result for relatively thick liquid films, e.g., $z>5d$ (see Fig. 3).

On the other hand, the exponential approximation to $\Pi(h)$ is given (in our notation) by

$$\Pi(h)\approx\Pi_s\exp(-(z-z_0)/l), \tag{31}$$

where $\Pi_s=(p_1-p_2)|_{\mu=\mu_s}$ is the disjoining pressure at the zero thickness ($z=z_0$), and l is the correlation length for the film near the solid particle. Clearly, l cannot be given from the classical heterogeneous nucleation theory. A fit of l to the DFT calculation yields $l\sim1.5d$. We also find l slightly increases with the temperature. Figure 3 shows that the exponential approximation to Π is in good agreement with Π calculated from the DFT for $z_0<z<5d$.

IV. CHEMICAL POTENTIAL OF THE LIQUID CONDENSATE

Calculation of the barrier height to nucleation requires the chemical potential of the liquid condensate as a function of the droplet's size R as well as the number of particles in the droplet or in the adsorbed film, ν. In this section, we will find the R- and ν-dependence based on the DFT model.

A. Chemical potential of liquid condensate and *R* dependence

We start from Eqs. (5) and (11). The surface tension $\sigma_{21}(R)$ appears in both equations. Since we consider only the condensation on mesoscopic solid particles, R is large enough to warrant the use of the Tolman formula[25]

$$\sigma_{21}=\sigma_{21}^{\infty}\left(1-\frac{2\delta_\infty}{R}\right), \tag{32}$$

where σ_{21}^{∞} is the surface tension of the planar liquid–vapor interface in the absence of the solid particle, and δ_∞ is the the Tolman length when $R\to\infty$. Previous DFT[26–28] has shown that (i) $\sigma_{21}(R)$ is not a monotonic function of R, (ii) σ_{21} approaches zero as $R\to0$, (iii) Eq. (32) is applicable only when R is at least greater than $5d$, and (iv) δ_∞ is a small negative constant. For the mesoscopic solid particle considered here, the condition $R>5d$ is well satisfied.

Taking the dividing surface to be the equimolar dividing surface so that $\Gamma_{21}=0$, and substituting Eq. (32) into Eq. (11) gives

$$\frac{\partial\sigma_{21}}{\partial R}=\frac{d\sigma_{21}}{dR}=\frac{d}{dR}\sigma_{21}^{\infty}\left(1-\frac{2\delta_\infty}{R}\right)=\frac{2\sigma_{21}^{\infty}\delta_\infty}{R^2}. \tag{33}$$

Substituting Eq. (33) into the Laplace equation (5) gives

$$p_2-p_1=\frac{2\sigma_{21}^{\infty}}{R}\left(1-\frac{\delta_\infty}{R}\right)-\Pi(h). \tag{34}$$

It is well known that the compressibility correction is in the same order as the curvature correction. Therefore, we should also take into account the compressibility corrections which were not included in the classical consideration.[2]

In Eq. (34), the pressure difference p_2-p_1 can be calculated via the compressibility route. We start from the density of the liquid, which can be given approximately by

$$\rho_2=\rho_{2\infty}+\rho_{2\infty}^2\chi_2\Delta\mu, \tag{35}$$

where $\rho_{2\infty}$ is the density of the uniform liquid at $\mu=\mu_\infty$, χ_2 is the compressibility of the liquid, and $\Delta\mu=\mu-\mu_\infty$. We can show from the DFT that Eq. (35) provides an accurate estimation for ρ_2 except when μ is very close to μ_s where the dependence ρ_2 on μ becomes nonlinear. Integrating Eq. (35) over μ yields the pressure of the liquid

$$p_2=p_{2\infty}+\rho_{2\infty}\Delta\mu+\tfrac{1}{2}\rho_{2\infty}^2\chi_2\Delta\mu^2, \tag{36}$$

where $p_{2\infty}$ is the pressure of the liquid at $\mu=\mu_\infty$, and $p_{2\infty}=p_{1\infty}$. Thus, the second formula for p_2-p_1 is

$$p_2-p_1=p_{1\infty}-p_1+\rho_{2\infty}\Delta\mu+\tfrac{1}{2}\rho_{2\infty}^2\chi_2\Delta\mu^2. \tag{37}$$

In Eq. (37), the term $p_{1\infty}-p_1$ can be neglected compared to the next two terms as $\rho_1\ll\rho_2$. The latter condition is satisfied for the LJ system at the reduced temperatures 0.7 and 0.9 since both are far below the critical temperature.

Combining Eq. (37) with Eq. (34) and neglecting $p_{1\infty}-p_1$ results in a quadratic equation (38) for $\Delta\mu$

$$\frac{1}{2}\rho_{2\infty}^2\chi_2\Delta\mu^2+\rho_{2\infty}\Delta\mu-\frac{2\sigma_{21}^{\infty}}{R}\left(1-\frac{\delta_\infty}{R}\right)+\Pi(h)=0. \tag{38}$$

Since δ_∞/R, $\sigma_{21}^{\infty}\chi_2/R$, and $\Pi\chi_2$ in Eq. (38) are all small parameters due to the mesoscopic size of the droplet R as well as the small value of compressibility of the liquid, the solution of the quadratic equation of $\Delta\mu$ can be expressed in terms of these small parameters to the first order, that is

$$\Delta\mu=\frac{1}{\rho_{2\infty}}\left[\frac{2\sigma_{21}^{\infty}}{R}\left(1-\frac{\delta_\infty+\sigma_{21}^{\infty}\chi_2}{R}+\Pi\chi_2\right)-\Pi-\frac{\chi_2}{2}\Pi^2\right]. \tag{39}$$

Equation (39) is an important result of this paper. It gives the chemical potential of liquid condensate as a function of the droplet size R, which will be used later to calculate the bar-

Downloaded 18 Apr 2007 to 129.93.16.206. Redistribution subject to AIP license or copyright, see http://jcp.aip.org/jcp/copyright.jsp

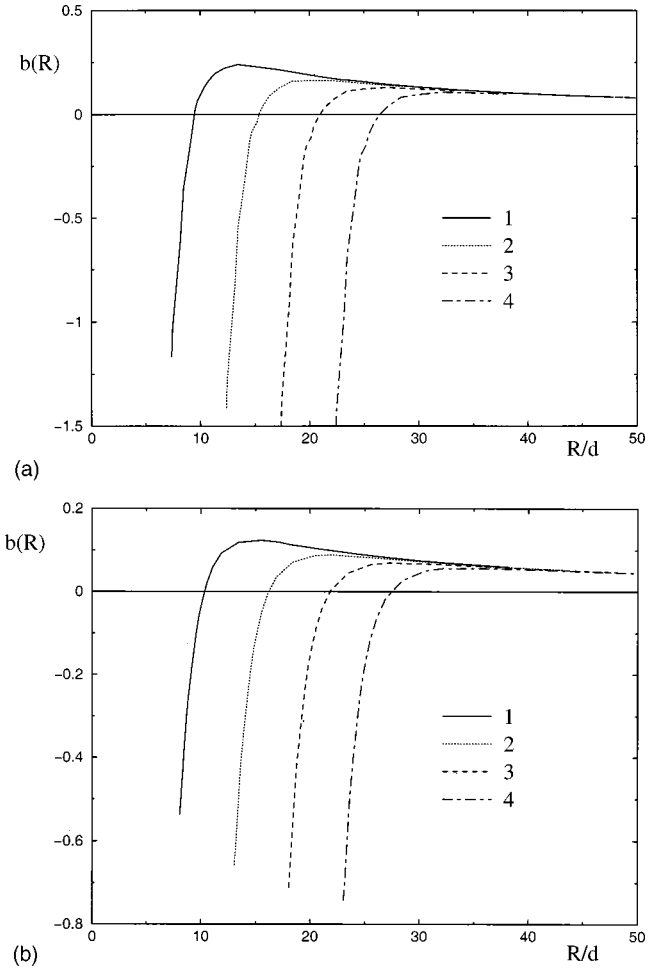

FIG. 4. Dependence of the scaled chemical potential $b(R)=\Delta\mu/k_BT$ of the liquid condensate on the scaled radius of the droplet R/d for various given radius $\tilde{R}_n$ of the solid particle; curve 1: $\tilde{R}_n=5d$, curve 2: $\tilde{R}_n=10d$, curve 3: $\tilde{R}_n=15d$, and curve 4: $\tilde{R}_n=20d$. (a) $T^*=0.7$; (b) $T^*=0.9$.

rier to nucleation. It can be reduced to the classical equation by removing curvature and compressibility corrections. Comparing the DFT results of $\Delta\mu(h)$ in the planar limit with those by using Eq. (39) (analytical planar expression based on the disjoining pressure and compressibility corrections) indicates that Eq. (39) provides quite a good estimation of the chemical potential as function of the film thickness. Indeed, at low temperatures the difference is negligible except for $h<1.5d$, for which the difference is still less than a few percent.

Note that several quantities in Eq. (39) can be obtained directly from experiments. These include the disjoining pressure $\Pi(h)$,[21] the liquid compressibility χ_2, the liquid density $\rho_{2\infty}$, and the planar surface tension σ_{21}^{∞}. Only the Tolman length δ_∞ has not yet been measured because it is on the order of molecular length scale. Of course, all these quantities can also be calculated from the DFT. Appendix A describes how the surface tension and the Tolman length can be determined based on the WDA-DFT. On the other hand the classical nucleation theory can only provide some estimation for the chemical potential $\Delta\mu$; neither $\Pi(h)$ nor σ_{21}^{∞} and δ_∞ can be determined in the framework of this theory.

Once the σ_{21}^{∞} and δ_∞ are determined from the WDA-DFT, the chemical potential of the liquid condensate as a function of droplet radius R can be evaluated from Eq. (39). Results are shown in Fig. 4 for $\tilde{R}_n>5d$. We find that the R dependence is not monotonic but has a maximum at a scaled chemical potential b_m at $R=R_m$ (hereafter, we use the dimensionless chemical potential $b\equiv\Delta\mu/k_BT$). Similar R dependence was found from the classical heterogeneous nucleation theory,[2,4] although empirical parameters were used.

Let b_1 be the dimensionless chemical potential of the metastable vapor. If $0<b_1<b_m$, the equation $b(R)=b_1$ has two solutions. One solution is $R=R_e$, for which $db(R)/dR>0$. It corresponds to a stable droplet of the liquid condensate forming on the solid particle, and this droplet is in chemical equilibrium with the surrounding supersaturated vapor. Another solution is at $R=R_c$, for which $db(R)/dR<0$. It corresponds to the critical droplet of the liquid condensate with the solid particle at the center, and this droplet is in unstable equilibrium with the surrounding supersaturated vapor. The equilibrium droplet cannot grow in size. To grow, the droplet size should be larger than R_c to overcome the barrier to nucleation. Finally, if $b_1>b_m$ the equation $b(R)=b_1$ does not have any solutions and the heterogeneous nucleation becomes barrierless.

We close this subsection by noting that at the maximum value of b the corresponding droplet size R_m is always in the region of thick films (see Fig. 4) for all solid particle sizes $\tilde{R}_n$ considered. Therefore, at R_m, the disjoining pressure $\Pi(R_m)$ can be well described by the power-law approximation [Eq. (29)].

B. The number of molecules ν in the liquid condensate and adsorbed film

Calculation of the barrier to droplet formation requires not only the R dependence of the chemical potential, but also the chemical potential as a function of the number of molecules ν in the liquid condensate or the adsorbed film as well.[2,4] In general, this number is given by

$$\nu=\frac{4\pi}{3}(R^3-R_n^3)\rho_2+4\pi R_n^2\Gamma_{32}+4\pi R^2\Gamma_{21}, \tag{40}$$

where ρ_2 can be determined from Eq. (35). Note that we have chosen the liquid–vapor dividing surface such that $\Gamma_{21}=0$. We have also chosen the solid–liquid dividing surface such that Γ_{32} is a constant for $R>R_n$. This constant can be found from Eqs. (25) and (26). For mesoscopic solid particles, we assume the adsorption Γ_{32} is the same as that in the planar case. However, for $R=R_n$, we know that $h=0$ and $\Gamma_{32}=\Gamma_{31}$ at $\mu=\mu_s$. If $\mu<\mu_s$, the adsorption Γ_{32} is not well defined and Γ_{31} cannot be considered as a constant. In fact, whenever $\mu<\mu_s$ and the film has a zero thickness ($h=0$), which means that the liquid condensate no longer exists except for an adsorbed film on the surface of the solid particle. Combining Eqs. (35), (39), and (40) and taking into account both liquid condensate and adsorbed film and keeping only first-order terms, we obtain

Downloaded 18 Apr 2007 to 129.93.16.206. Redistribution subject to AIP license or copyright, see http://jcp.aip.org/jcp/copyright.jsp

$$\nu(R)=\frac{4\pi}{3}(R^3-R_n^3)\rho_{2\infty}\left(1+\rho_{2\infty}\chi_2\left(\frac{2\sigma_{21}^{\infty}}{R}-\Pi(h)\right)\right)+4\pi R_n^2\Gamma_{32},\quad R>R_n$$
$$\nu(\Gamma_{31})=4\pi R_n^2\Gamma_{31},\quad R=R_n. \tag{41}$$

Consequently, for $\mu<\mu_s$, ν no longer depends on R but only on Γ_{31}, which changes from zero to a finite value when $h=0$.

C. Dependence of ν on the gas adsorption Γ_{31}

For the planar solid surface ($R_n\to\infty$), the gas adsorption Γ_{31} can be calculated for given $\mu<\mu_s$ from the equation

$$\Gamma_{31}(\mu)=\int_0^{\tilde{L}}\rho(z)dz-\rho_1(\tilde{L}-z_0), \tag{42}$$

where z_0 is the position of the dividing surface. Meanwhile, the pressure of an undersaturated vapor, p_1, can be calculated from Eq. (21), or approximately from the ideal-gas law because ρ_1 is very small. Combining Eq. (21) with Eq. (42) for μ gives the gas-adsorption isotherm $p_1=g(\Gamma_{31})$, where g is some function of Γ_{31}. Figure 5 shows Γ_{31} versus ρ_1 (for the ideal gas ρ_1 and the scaled pressure p_1/k_BT are the same), which shows Γ_{31} is a stepwise monotonic function. This type of isotherm has been classified by earlier workers as one of the several typical isotherms[29] for the gas adsorption on the solid surface. The stepwise nature of this isotherm stems from the oscillatory behavior of the density profile of the adsorbed film. Note that in the classical theory the linear or Henry's law isotherm was used,[5] that is,

$$\Gamma_{31}=K_\Gamma\rho_1, \tag{43}$$

where K_Γ is the Henry's law constant.

In the case of $R=R_n$ and $\mu<\mu_s$, the grand potential of the system is given by

$$\Omega=-p_1\frac{4\pi}{3}(L^3-R_n^3)+4\pi R_n^2\sigma_{31}, \tag{44}$$

where $\sigma_{31}(R_n)=\sigma_{31}(\tilde{R}_n,z_0)$ is the surface tension of solid–vapor interface, which depends on both the curvature of the particle $\tilde{R}_n$ and the position of the dividing surface z_0. Since Ω itself is independent on the choice of z_0, taking derivative over z_0 on Eq. (44) gives

$$p_1=-\frac{2\sigma_{31}}{R_n}-\frac{\partial\sigma_{31}}{\partial z_0}. \tag{45}$$

Equation (45) is analog to the Laplace equation for liquid–vapor surfaces. We assume the two variables of $\sigma_{31}(\tilde{R}_n,z_0)$ are separable, i.e., $\sigma_{31}(\tilde{R}_n,z_0)=\sigma_{31}^{\infty}(z_0)c(\tilde{R}_n)$, which becomes exact as $\tilde{R}_n\to\infty$ where the function $c(\tilde{R}_n)$ approaches 1. Thus, for the planar solid surface ($R_n\to\infty$), Eq. (45) becomes

$$p_1=-\frac{\partial\sigma_{31}^{\infty}}{\partial z_0}, \tag{46}$$

or

$$g(\Gamma_{31})=-\frac{\partial\sigma_{31}^{\infty}}{\partial z_0}, \tag{47}$$

since $p_1=g(\Gamma_{31})$. Combining Eq. (47) with Eq. (45) gives

$$p_1=-\frac{2\sigma_{31}}{R_n}+c(\tilde{R}_n)g(\Gamma_{31}). \tag{48}$$

Moreover, because the vapor is in equilibrium with the adsorbed film, we have $p_1=p_{1\infty}\exp(b(\nu))$, assuming the vapor is an ideal gas. Here, $b(\nu)$ is the scaled chemical potential of the adsorbed film. Combining the equilibrium equation with Eq. (48), we obtain

$$b(\nu)=\ln\left(-\frac{2\sigma_{31}}{R_np_{1\infty}}+\frac{c(\tilde{R}_n)g(\Gamma_{31})}{p_{1\infty}}\right). \tag{49}$$

In Eq. (49), two unknowns remain to be determined: (1) σ_{31} and (2) $c(\tilde{R}_n)$. First, combining Eqs. (44) and (45) with the thermodynamic relation $d\Omega=-N\,d\mu=-(N_1+N_{31})d\mu$ and $dp_1=\rho_1\,d\mu$ results in

$$d\sigma_{31}=\frac{\partial\sigma_{31}}{\partial z_0}dR_n-\Gamma_{31}\,d\mu. \tag{50}$$

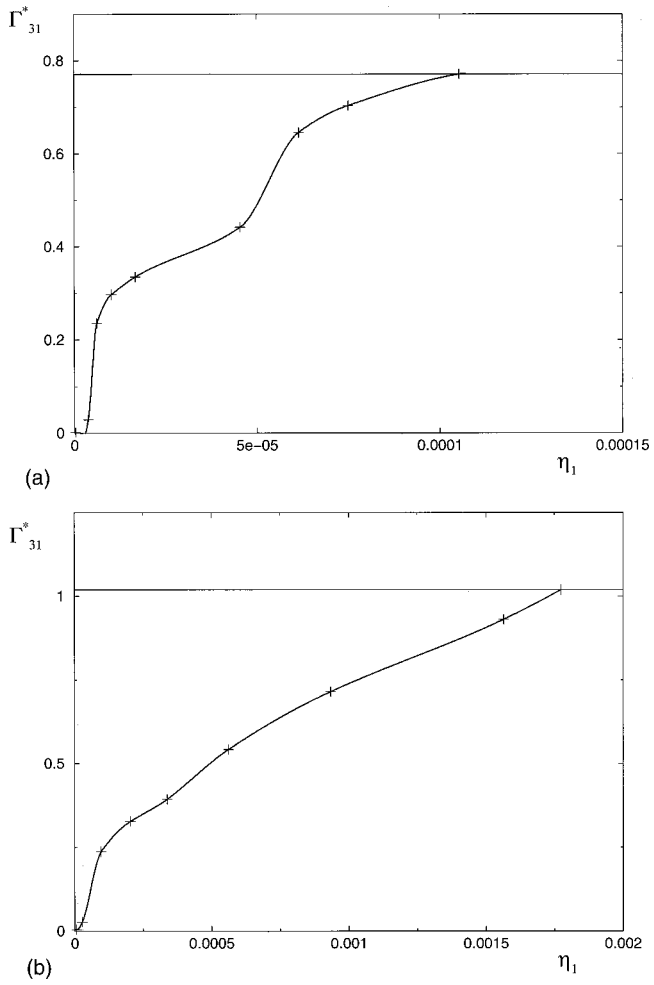

FIG. 5. Adsorption isotherms for the LJ fluid near the planar solid surface. The scaled adsorption $\Gamma_{31}^*=\Gamma_{31}\pi d^2/6$ vs scaled vapor density $\eta_1=\rho_1\pi d^3/6$. The horizontal line shows the value of Γ_{32}^*. (a) $T^*=0.7$; (b) $T^*=0.9$.

Downloaded 18 Apr 2007 to 129.93.16.206. Redistribution subject to AIP license or copyright, see http://jcp.aip.org/jcp/copyright.jsp

Because the size of the solid particle and the position of the dividing surface is fixed, Eq. (50) is reduced to

$$d\sigma_{31} = -\Gamma_{31} k_B T\, db(\nu). \tag{51}$$

Using Eqs. (49) and (51), we eliminate the first unknown, σ_{31}, and obtain a differential equation for $b(\nu)$

$$\frac{db(\nu)}{d\Gamma_{31}} = \frac{c(\tilde{R}_n)}{p_{1\infty}} \frac{dg(\Gamma_{31})}{d\Gamma_{31}} \frac{1}{\exp(b(\nu)) - 2\Gamma_{31}/R_n\rho_{1\infty}}, \tag{52}$$

where $\nu = 4\pi R_n^2 \Gamma_{31}$ [see Eq. (41)]. Next, we determine $c(\tilde{R}_n)$. To this end, we follow the method introduced in Ref. 5 by using the so-called patching condition $db(\nu)/d\nu|_{\Gamma_{31}=\Gamma_{32}} = db(\nu)/d\nu|_{R=R_n}$. The derivation of $c(\tilde{R}_n)$ is given in Appendix B.

Note that if the Henry's law isotherm is substituted for $g(\Gamma_{31})$ (which was used in the classical nucleation theory) Eq. (52) will have a simple analytic solution, $b(\nu) = \ln(a(\tilde{R}_n)\Gamma_{31})$, where the constant $a(\tilde{R}_n)$ can be determined with the same patching condition (see Appendix B). In reality, however, $g(\Gamma_{31})$ is not exactly a linear function but can be viewed approximately as some weak oscillations about a straight line (see Fig. 5). With this picture in mind, it is reasonable to express the solution of Eq. (52) as

$$b(\nu) = \ln(a(\tilde{R}_n)\Gamma_{31}) + \kappa(\Gamma_{31}), \tag{53}$$

where $\kappa(\Gamma_{31})$ represents a perturbation function which gives rise to the oscillations about the straight line. Let $\kappa(\Gamma_{31})|_{\Gamma_{31}=\Gamma_{32}} = 0$; the constant $a(\tilde{R}_n)$ can then be determined from patching condition, that is, $b(\nu)|_{R=R_n} = \ln(a(\tilde{R}_n)\Gamma_{32})$. Taking the assumed perturbative solution (53) into the differential equation (52) leads to a differential equation for $\kappa(\Gamma_{31})$

$$\frac{d\kappa(\Gamma_{31})}{d\Gamma_{31}} = \frac{1}{\Gamma_{31}}\left[\frac{c(\tilde{R}_n)}{p_{1\infty}} \frac{dg(\Gamma_{31})}{d\Gamma_{31}} \times \frac{1}{a(\tilde{R}_n)\exp(\kappa(\Gamma_{31})) - 2/(R_n\rho_{1\infty})} - 1\right]. \tag{54}$$

This equation is easier to solve than Eq. (52) as the latter contains a near-divergent term $\ln(a(\tilde{R}_n)\Gamma_{31})$. Numerical solution of Eq. (54) is obtained as well as that of $(b(\nu))$ of Eq. (53).

With both Eq. (39) for $\nu \geqslant 4\pi R_n^2 \Gamma_{32}$ and Eq. (53) for $\nu = 4\pi R_n^2 \Gamma_{31} \leqslant 4\pi R_n^2 \Gamma_{32}$, we obtain the chemical potential $b(\nu)$ over the entire range of ν. Figure 6 shows a plot of b versus ν for given R_n and temperatures, where $\nu = 0$ corresponds to the bare solid particle. For adsorbed films, weak oscillations appear on the $b(\nu)$ curves [see Figs. 6(a) and 6(c)], due to the stepwise structure of the adsorption isotherm. For thicker liquid films, these oscillations do not appear.

D. Chemical potential for barrierless and near-threshold nucleation

As mentioned above, a key feature in the $b(R)$ or $b(\nu)$ curves [Figs. 6(b) and 6(d)], is the existence of a maximum b_m at R_m or ν_m. For the purpose of discussing heterogeneous nucleation, let us define the threshold value $b_{th} = b_m$ of chemical potential of the vapor. In the overthreshold region $b_1 > b_{th}$, the heterogeneous nucleation process becomes barrierless. In the underthreshold region $0 < b_1 < b_{th}$, the barrier height to nucleation depends on the value of b_1. In practice, however, the near-threshold region in which b_1 is close to b_{th} has received more attention[2] because in this region the rate of nucleation can be conveniently measured.

A description of the near-threshold region has been given in Refs. 2 and 4. Following Ref. 2, we will use an ϵ parameter $(0 < \epsilon \ll 1)$ to characterizes how far b_1 is from b_{th}, that is,

$$b_1 = b_{th}(1 - \epsilon). \tag{55}$$

The barrierless nucleation occurs when $\epsilon = 0$ while the near-threshold nucleation is denoted by $\epsilon \ll 1$. In this region the chemical potential of the liquid condensate can be expanded up to the second order (the parabolic approximation[2,4]) about ν_m

$$b(\nu) = b_{th} - \frac{1}{2}\left|\frac{d^2 b(\nu)}{d\nu^2}\right|_{\nu_m} (\nu - \nu_m)^2, \tag{56}$$

where the first-order term vanishes because $db(\nu)/d\nu|_{\nu_m} = 0$. Validity of the parabolic approximation can be examined from the condition

$$\frac{1}{3}\left|\frac{(\nu - \nu_m) d^3 b(\nu)/d\nu^3|_{\nu_m}}{d^2 b(\nu)/d\nu^2|_{\nu_m}}\right| \ll 1, \tag{57}$$

that is, when the third-order term is much smaller than the second one. With the parabolic approximation, the number of molecules for a given ϵ in the equilibrium and critical droplet are given by

$$\begin{aligned} \nu_e &= \nu_m - (2\epsilon b_{th}/|d^2 b(\nu)/d\nu^2|_{\nu_m})^{1/2}, \\ \nu_c &= \nu_m + (2\epsilon b_{th}/|d^2 b(\nu)/d\nu^2|_{\nu_m})^{1/2}, \end{aligned} \tag{58}$$

respectively, and with which the condition Eq. (57) becomes

$$\frac{1}{3}(2\epsilon b_{th})^{1/2}\left|\frac{d^3 b(\nu)/d\nu^3|_{\nu_m}}{(d^2 b(\nu)/d\nu^2)^{3/2}|_{\nu_m}}\right| \ll 1. \tag{59}$$

Equations (55)–(59) form the basis for the description of the near-threshold region in the classical theory of heterogeneous nucleation.

Let us first determine ν_m or R_m from $db(\nu)/d\nu|_{\nu_m} = 0$ or from $db(R)/dR|_{R_m} = 0$ with using Eq. (39). Note again that Eq. (39) involves a zero-order term as well as first-order terms of compressibility and curvature. To separate their contribution to R_m, we write

$$R_m = R_m^{(0)}(1 + \zeta), \tag{60}$$

where $R_m^{(0)}$ denotes the solution of the equation with only the zero-order term, that is,

$$\frac{d}{dR}\left(\frac{2\sigma_{21}^{\infty}}{R} - \Pi\right) = -\frac{2\sigma_{21}^{\infty}}{R_m^2} - \left.\frac{\partial \Pi}{\partial z}\right|_{R=R_m^{(0)}} = 0. \tag{61}$$

Downloaded 18 Apr 2007 to 129.93.16.206. Redistribution subject to AIP license or copyright, see http://jcp.aip.org/jcp/copyright.jsp

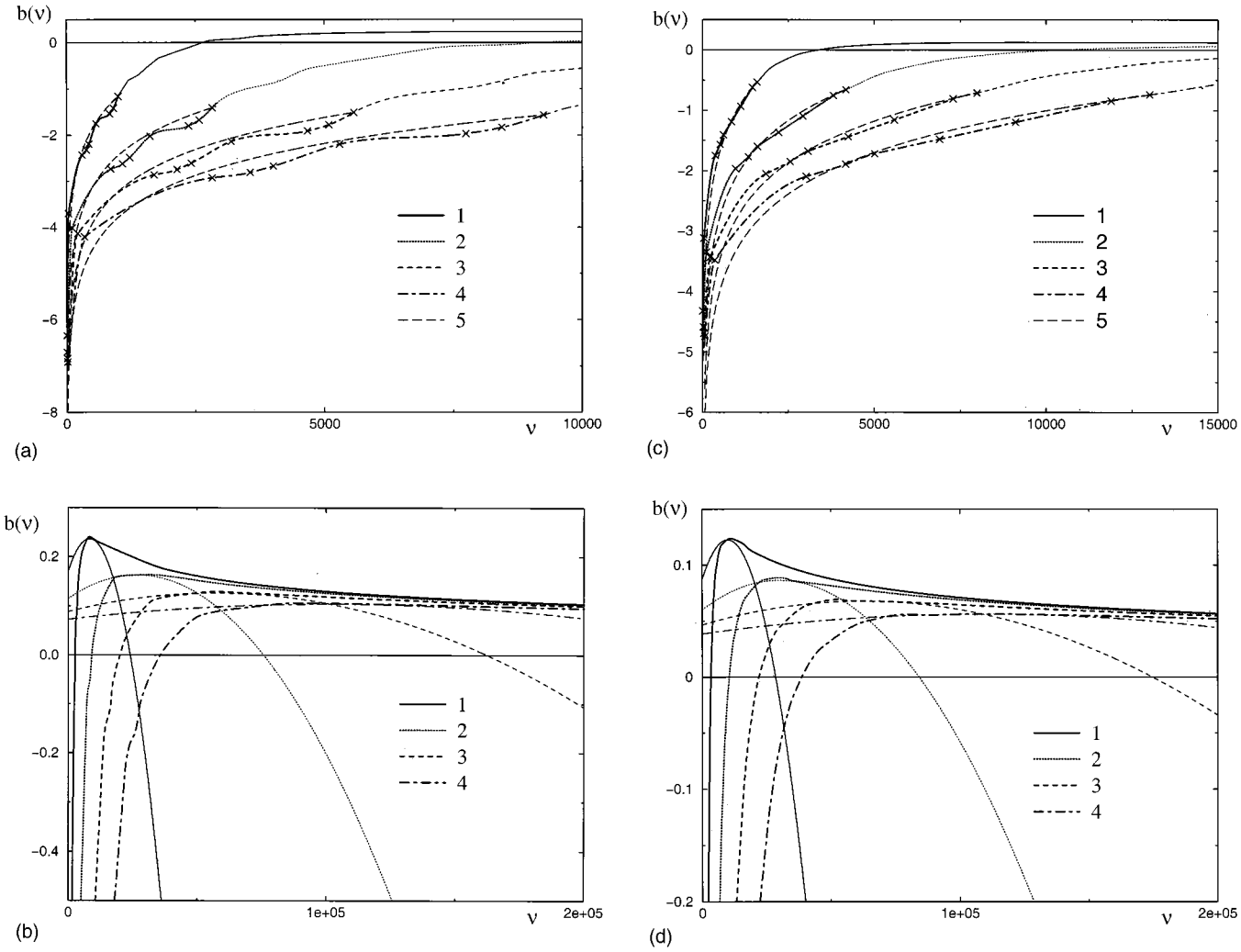

FIG. 6. Dependence of the scaled chemical potential $b(\nu)$ of the liquid condensate on the number of particles ν in the condensate; curve 1: $\tilde{R}_n=5d$, curve 2: $\tilde{R}_n=10d$, curve 3: $\tilde{R}_n=15d$, and curve 4: $\tilde{R}_n=20d$. (a) and (b): $T^*=0.7$; (c) and (d): $T^*=0.9$. Curve 5 in (a) and (c) represents the classical approximation $b(\nu)=\ln(a(\tilde{R}_n)\Gamma_{31})$. The thinner curves in (b) and (d) represent the parabolic approximation.

ζ is a small correction to $R_m^{(0)}$ by including the first-order terms in Eq. (39). Substituting Eq. (60) with the solution $R_m^{(0)}$ from Eq. (61) into $db(R)/dR|_{R_m}=0$ gives

$$\zeta=-\frac{4\sigma_{21}^{\infty}\delta_{\infty}}{R_m^{(0)4}(4\sigma_{21}^{\infty}/R_m^{(0)3}-\partial^2\Pi/\partial z^2|_{R_m^{(0)}})}. \tag{62}$$

Next, since R_m is in the region of thick films (Sec. IV A), the power-law approximation [Eq. (29)] can be used to evaluate Π in Eq. (61). As a result, the positive solution of the quadratic equation (61) is

$$R_m^{(0)}=\tilde{R}_n+\frac{1}{2}\sqrt{\frac{3B}{2\sigma_{21}^{\infty}}}+\sqrt{\tilde{R}_n\sqrt{\frac{3B}{2\sigma_{21}^{\infty}}}+\frac{3B}{8\sigma_{21}^{\infty}}}. \tag{63}$$

Substituting this zero-order solution into Eq. (62) gives the first-order correction

$$\zeta=\frac{\delta_{\infty}}{R_m^{(0)}}\frac{R_m^{(0)}-\tilde{R}_n}{R_m^{(0)}+\tilde{R}_n}. \tag{64}$$

Finally, substituting Eqs. (60) and (64) into Eq. (41) gives

$$\begin{aligned}\nu_m&=4\pi R_n^2\Gamma_{32}+\frac{4\pi}{3}\rho_{2\infty}(R_m^{(0)3}-R_n^3+3\zeta R_m^{(0)3})\\&\quad\times\left(1+\chi_2\left(\frac{2\sigma_{21}^{\infty}}{R_m^{(0)}}-\Pi|_{R=R_m^{(0)}}\right)\right)\\&=4\pi R_n^2\Gamma_{32}+\frac{4\pi}{3}\rho_{2\infty}(R_m^{(0)3}-R_n^3)\\&\quad\times\left(1+\frac{3(R_m^{(0)}-\tilde{R}_n)R_m^{(0)2}}{(R_m^{(0)}+\tilde{R}_n)(R_m^{(0)3}-R_n^3)}\delta_{\infty}\right.\\&\quad\left.+\chi_2\frac{2\sigma_{21}^{\infty}}{R_m^{(0)}}\frac{2R_m^{(0)}+\tilde{R}_n}{3R_m^{(0)}}\right).\end{aligned} \tag{65}$$

Using $R_m^{(0)}$ [Eq. (63)] and Eq. (29), we obtain the threshold chemical potential

Downloaded 18 Apr 2007 to 129.93.16.206. Redistribution subject to AIP license or copyright, see http://jcp.aip.org/jcp/copyright.jsp

$$b_{th}=\frac{1}{\rho_{2\infty}k_BT}\frac{2\sigma_{21}^{\infty}}{R_m^{(0)}}\frac{2R_m^{(0)}+\tilde{R}_n}{3R_m^{(0)}}\left(1-\frac{3\delta_\infty}{2R_m^{(0)}+\tilde{R}_n}-\frac{3\sigma_{21}^{\infty}\chi_2}{2R_m^{(0)}+\tilde{R}_n}\frac{4R_m^{(0)2}+4R_m^{(0)}\tilde{R}_n+\tilde{R}_n^2}{9R_m^{(0)2}}\right). \tag{66}$$

Having derived ν_m, the validity condition of the parabolic approximation [Eq. (56)] can be examined by calculating the second and third derivative of $b(\nu)$ at ν_m. Detailed expressions are given in Appendix C. Moreover, given Eqs. (66) and (C2), we can calculate the size of equilibrium cluster ν_e and critical cluster ν_c using Eq. (58). In Fig. 6, the parabolic approximation of $b(\nu)$ [Eq. (56)] is also shown for the given $\tilde{R}_n$ and temperatures. One can see that the approximation is quite good, particularly near $\nu=\nu_m$, which is the near-threshold region in which we are interested.

V. FREE ENERGY OF DROPLET FORMATION AND THE BARRIER HEIGHT

The free energy of droplet formation and barrier height are key characteristics that control the rate of nucleation. In the last section we have derived the chemical potential as a function of the number of molecules $b(\nu)$. This relation will be used to calculate the free energy of droplet formation.

A. Free energy of droplet formation $W(\nu)$

On the basis of nucleation thermodynamics,[30] we know that if a liquid droplet is in mechanical and thermal equilibrium with the surrounding vapor, we have

$$\partial W/\partial\nu=b(\nu)-b_1, \tag{67}$$

where W is the free energy of droplet formation in unit of k_BT. Integrating Eq. (67) using the boundary condition $W(0)=0$ (the formation free energy is zero for a bare solid particle) gives

$$W(\nu)=\int_0^{\nu}d\tilde{\nu}(b(\tilde{\nu})-b_1). \tag{68}$$

Note that our definition of ν differs slightly from that in Ref. 2 by a value ν_n. The latter is the number of molecules of the liquid condensate required to fill the volume of solid particle. Because we consider liquid compressibility, ν_n cannot be treated as a constant. Substituting $d\tilde{\nu}$ [from Eq. (41)] into Eq. (68) gives

$$W(\nu)=4\pi R_n^2\int_0^{\Gamma_{32}}b(\nu)d\Gamma_{31}+4\pi\int_{R_n}^{R}dR\,\rho_{2\infty}b(R)\times\left[1+\chi_2k_BT\rho_{2\infty}\left(b(R)+\frac{1}{3}\frac{R^3-R_n^3}{R^2}\frac{db(R)}{dR}\right)\right]-b_1\nu, \tag{69}$$

where $b(R)$ is given by Eq. (39) and $b(\nu)$ by Eq. (53). Again, keeping only the first-order terms of curvature and compressibility, we have

$$W(\nu)=4\pi R_n^2\int_0^{\Gamma_{32}}b(\nu)d\Gamma_{31}+\frac{4\pi}{k_BT}\int_{R_n}^{R}dR\times\left[R^2\left(\frac{2\sigma_{21}^{\infty}}{R}\left(1-\frac{\delta_\infty-1/3\sigma_{21}^{\infty}\chi_2}{R}-\frac{2}{3}\Pi\chi_2\right)-\Pi+\frac{\chi_2}{2}\Pi^2\right)+\frac{(R^3-R_n^3)\chi_2}{3}\left(\Pi\frac{d\Pi}{dR}-\frac{2\sigma_{21}^{\infty}}{R}\frac{d\Pi}{dR}\right)+\frac{R_n^3\chi_2 2\sigma_{21}^{\infty}}{3R^2}\left(\frac{2\sigma_{21}^{\infty}}{R}-\Pi\right)\right]-b_1\nu. \tag{70}$$

The two integrals involving $d\Pi/dR$ can be further evaluated using the integration by parts, that is,

$$\begin{aligned}&4\pi\chi_2\int_{R_n}^{R}R^2\frac{R}{3}\Pi\frac{d\Pi}{dR}\\&\quad=\frac{4\pi}{3}\chi_2\left(\frac{R^3}{2}\Pi^2|_{R_n}^{R}-\frac{3}{2}\int_{R_n}^{R}R^2\Pi^2\,dR\right),\\&-4\pi\chi_2\int_{R_n}^{R}R^2\frac{2}{3}\sigma_{21}^{\infty}\frac{d\Pi}{dR}\\&\quad=-4\pi\sigma_{21}^{\infty}\chi_2\frac{2}{3}R^2\Pi|_{R_n}^{R}+4\pi\sigma_{21}^{\infty}\chi_2\frac{2}{3}\int_{R_n}^{R}2R\Pi\,dR.\end{aligned} \tag{71}$$

With Eq. (71), Eq. (70) becomes

$$W(\nu)=4\pi R_n^2\int_0^{\Gam_{32}}b(\nu)d\Gamma_{31}+\frac{4\pi R^2\sigma_{21}^{\infty}}{k_BT}\left(1-\frac{2\delta_\infty}{R}\right)\Bigg|_{R_n}^{R}+\frac{4\pi}{3}(R^3-R_n^3)\frac{\chi_2}{2k_BT}\left(\frac{2\sigma_{21}^{\infty}}{R}-\Pi|_{h=R-R_n}\right)^2-\frac{4\pi}{k_BT}\int_{R_n}^{R}R^2\Pi\,dR-b_1\nu. \tag{72}$$

This expression of $W(\nu)$ can be reduced to the classical one[2] if the first-order curvature and compressibility corrections are removed and if the adsorption term is included in Π. Finally, we obtain the following expression for the free energy of droplet formation on the solid particle in the case of $\nu>4\pi R_n^2\Gamma_{32}$:

$$W(\nu)=4\pi R_n^2\left[\Gamma_{32}(\ln(a(\tilde{R}_n)\Gamma_{32})-1)+\int_0^{\Gamma_{32}}\kappa(\Gamma_{31})d\Gamma_{31}\right]+\frac{4\pi R^2\sigma_{21}^{\infty}}{k_BT}\left(1-\frac{2\delta_\infty}{R}\right)\Bigg|_{R_n}^{R}+\frac{4\pi}{3}(R^3-R_n^3)\frac{\chi_2}{2k_BT}\left(\frac{2\sigma_{21}^{\infty}}{R}-\Pi|_{h=R-R_n}\right)^2-\frac{4\pi}{k_BT}\int_{R_n}^{R}R^2\Pi\,dR-b_1\nu. \tag{73}$$

For $\nu<4\pi R_n^2\Gamma_{32}$, we have

Downloaded 18 Apr 2007 to 129.93.16.206. Redistribution subject to AIP license or copyright, see http://jcp.aip.org/jcp/copyright.jsp

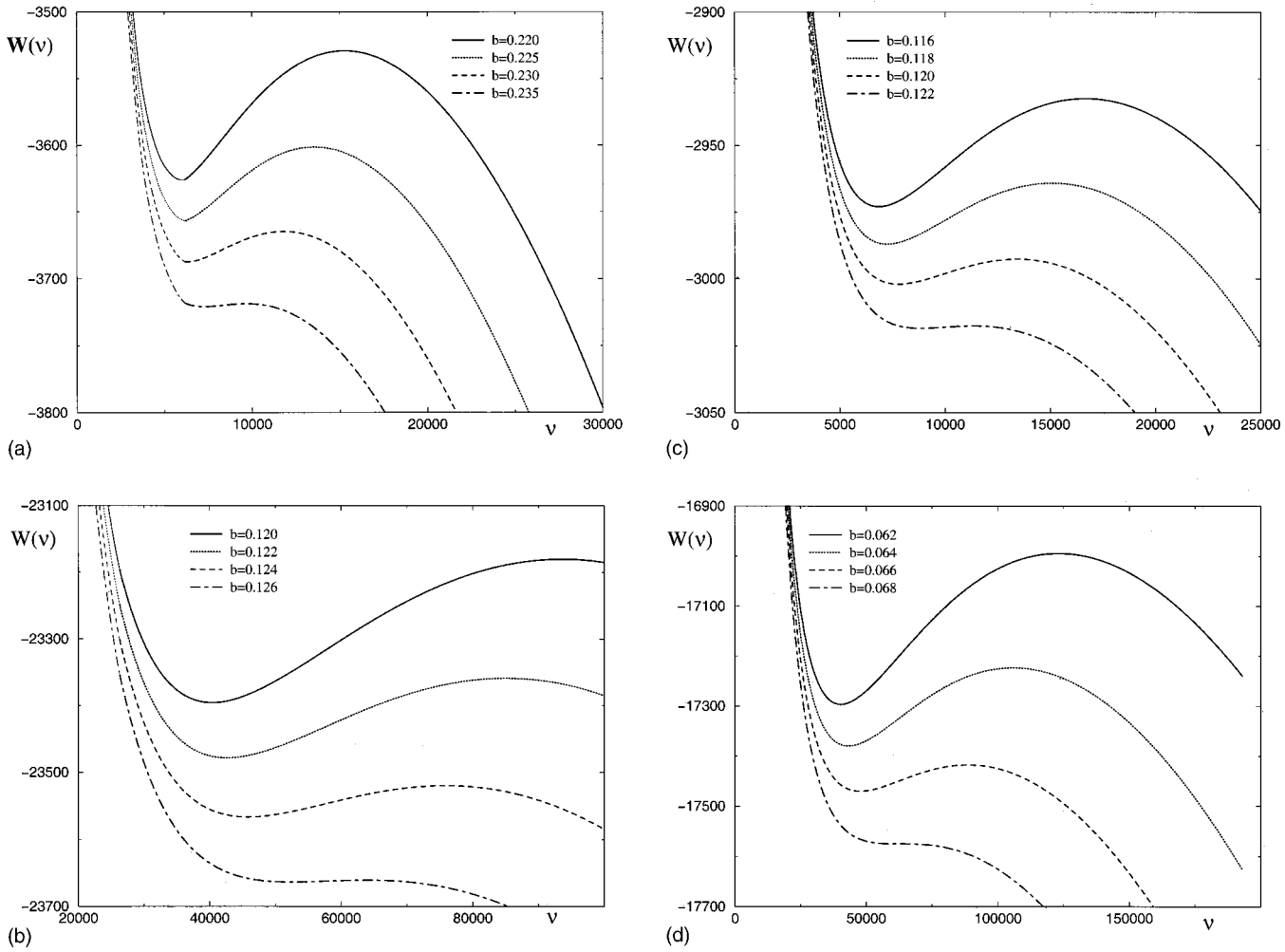

FIG. 7. Dependence of the scaled free energy of droplet formation $W(\nu)$ on the number of molecules ν for various given chemical potentials (or supersaturations). (a) and (c): $\tilde{R}_n=5d$; (b) and (d): $\tilde{R}_n=15d$. (a) and (b): $T^*=0.7$; (c) and (d): $T^*=0.9$. The thicker curves represent the region where the power-law approximation is applicable.

$$W(\nu)=4\pi R_n^2\left[\Gamma_{31}(\ln(a(\tilde{R}_n)\Gamma_{31})-1)+\int_0^{\Gamma_{31}}\kappa(\tilde{\Gamma}_{31})d\tilde{\Gamma}_{31}\right]-b_1\nu. \tag{74}$$

For the limiting case of $R_n=0$ and $\Pi=0$, Eq. (73) will be reduced to

$$W_{\text{homog}}(\nu)=\frac{4\pi R^2\sigma_{21}^{\infty}}{k_BT}\left(1-\frac{2\delta_{\infty}}{R}\right)+\frac{4\pi}{3}R^3\frac{\chi_2}{2k_BT}\left(\frac{2\sigma_{21}^{\infty}}{R}\right)^2-b_1\nu, \tag{75}$$

which indeed is the free energy of droplet formation for homogeneous nucleation. Therefore, the difference $W(\nu)-W_{\text{homog}}(\nu)$ can be identified as the work of wetting, which is entirely due to the presence of the solid particle.

To calculate the integrals in Eq. (73) we used numerical results for $\Pi(h)$ up to a certain value of R, and beyond that R we used the power-law approximation [Eq. (29)]. Results of $W(\nu)$ for given b_1 and R_n are shown in Fig. 7. All the $W(\nu)$ curves exhibit the ''loop'' behavior which is typical for heterogeneous nucleation. Similar behavior has been predicted from the classical theory, but only qualitatively because the theory utilizes numerous empirical parameters. The minimum on these curves corresponds to the equilibrium size ν_e, at which the solid particle is covered by a liquid film with a finite thickness and in stable equilibrium with the surrounding supersaturated vapor. The value $W_e=W(\nu_e)$ is negative, which means the formation of the equilibrium liquid film is spontaneous but it cannot grow further into a liquid droplet. The maximum at ν_c on the $W(\nu)$ curves corresponds to the peak of the barrier.

B. The barrier height to nucleation ΔW

The height of the barrier is defined as $\Delta W\equiv W(\nu_c)-W(\nu_e)$. Typically, ΔW is no greater than several tens of k_BT for which the nucleation rate is measurable. If $\nu>\nu_c$ the size of the droplet is large enough to overcome the barrier to nucleation. As $b_1\to b_{th}$ from below, both ν_e and ν_c approach to ν_m. As we know, ν_m depends on R_n but not on the supersaturation characterized by b_1. This means that whenever $b_1=b_{th}$, $\Delta W(\nu_m)=0$, that is, the nucleation becomes barrierless.

Downloaded 18 Apr 2007 to 129.93.16.206. Redistribution subject to AIP license or copyright, see http://jcp.aip.org/jcp/copyright.jsp

As discussed in Sec. IV, we are particularly interested in the near-threshold region, where the nucleation barrier is less than a few tens of k_BT (see Fig. 7). It has been shown in Ref. 2 that in the near-threshold region the parabolic approximation [Eq. (56)] to $b(\nu)$ is valid, and thus Eq. (68) becomes

$$\Delta W=\int_{\nu_e}^{\nu_c} d\nu(b(\nu)-b) =\frac{4}{3}\epsilon^{3/2}b_{th}^{3/2}\left[\frac{2}{|d^2b(\nu)/d\nu^2|_{\nu_m}}\right]^{1/2}. \tag{76}$$

Moreover, in the region near ν_e and ν_c one has

$$W=W_e+\left[\frac{(\nu-\nu_e)}{\Delta\nu_e}\right]^2, \quad W=W_c-\left[\frac{(\nu-\nu_c)}{\Delta\nu_c}\right]^2, \tag{77}$$

where $\Delta\nu_e$ and $\Delta\nu_c$ are the half width of the minimum and maximum on the $W(\nu)$ curve, respectively, and are given by

$$\Delta\nu_e=\Delta\nu_c=\left(\frac{2}{\epsilon b_{th}d^2b(\nu)/d\nu^2|_{\nu_m}}\right)^{1/4}. \tag{78}$$

Using b_{th} [Eq. (66)] and $|d^2b(\nu)/d\nu^2|_{\nu_m}$ [Eq. (C2)] obtained in this work and substituting them into Eq. (76), keeping only first-order terms of curvature and compressibility, gives

$$\Delta W=\frac{8}{3}\frac{\epsilon^{3/2}}{k_BT}4\pi R_m^{(0)2}\sigma_{21}^{\infty}\left(\frac{2R_m^{(0)}+\tilde{R}_n}{3R_m^{(0)}}\right)^{3/2}\left(\frac{R_m^{(0)}-\tilde{R}_n}{R_m^{(0)}+\tilde{R}_n}\right)^{1/2} \times\left(1+\frac{\delta_\infty}{2R_m^{(0)}}\frac{7R_m^{(0)3}+2R_m^{(0)2}\tilde{R}_n-11R_m^{(0)}\tilde{R}_n^2-4\tilde{R}_n^3}{(R_m^{(0)}+\tilde{R}_n)^2(2R_m^{(0)}+\tilde{R}_n)} +\frac{\sigma_{21}^{\infty}\chi_2}{2R_m^{(0)2}}\frac{4R_m^{(0)2}+4R_m^{(0)}\tilde{R}_n+\tilde{R}_n^2}{2R_m^{(0)}+\tilde{R}_n}\right). \tag{79}$$

In Fig. 8 we plot ΔW as a function of parameter ϵ for given $\tilde{R}_n$. Two sets of curves can be seen in Fig. 8. The first is obtained by using $\Delta W=W(\nu_c)-W(\nu_e)$ with the numerical results shown in Fig. 7. The second is obtained by using Eq. (79) with $\epsilon\ll 0.08$ (in the near-threshold region). The fact that both sets of curves show very good agreement indicates Eq. (79) indeed gives quite accurate prediction on the barrier height in the near-threshold region. Furthermore, if the curvature and compressibility corrections are neglected [in Eq. (79)] and if Eq. (79) is expanded over the small thickness of the film, $R_m^{(0)}-\tilde{R}_n$, the classical formula (7.16) in Ref. 2 will be reproduced. This result shows that our approach can recover not only results of the classical theory, but also evaluate the extent to which those approximations underlying the classical theory are applicable.

The half-width $\Delta\nu_e$ and $\Delta\nu_c$ can be calculated for our model via combining Eqs. (66) and (C2) with Eq. (78), which gives

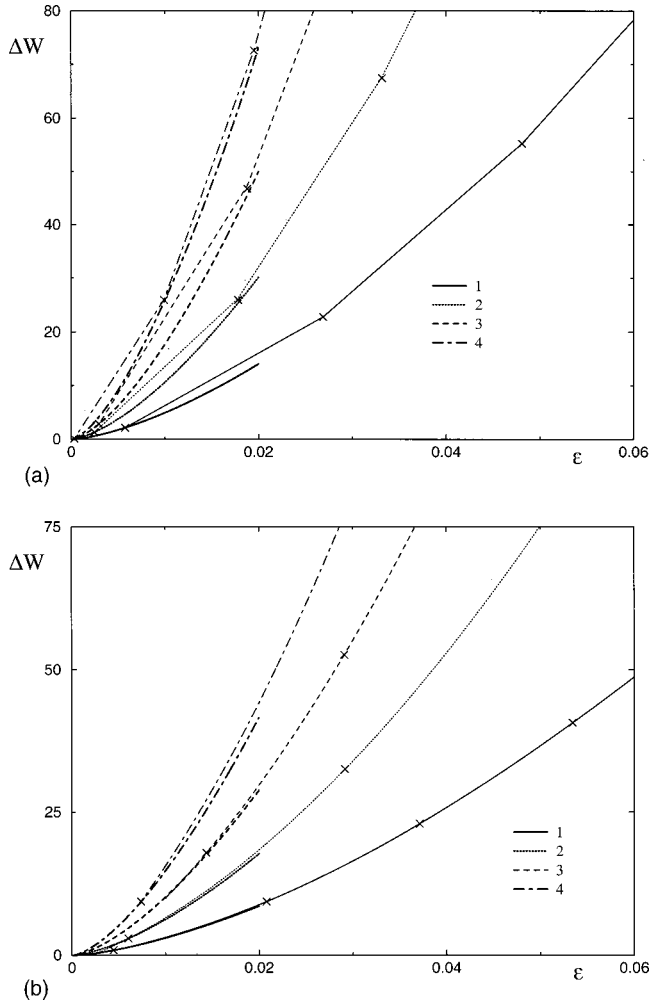

FIG. 8. Dependence of the scaled barrier height ΔW on the ϵ parameter; curve 1: $\tilde{R}_n=5d$, curve 2: $\tilde{R}_n=10d$, curve 3: $\tilde{R}_n=15d$, and curve 4: $\tilde{R}_n=20d$. (a) $T^*=0.7$; (b) $T^*=0.9$. The thicker curves result from Eq. (79), whereas the thinner curves result from numerical integration of the chemical potential shown in Fig. 6.

$$\Delta\nu_e=\Delta\nu_c=\frac{\rho_{2\infty}R_m^{(0)2}}{\epsilon^{1/4}}\left(\frac{2\pi k_BT}{\sigma_{21}^{\infty}}\right)^{1/2}\left(\frac{3R_m^{(0)}}{2R_m^{(0)}+\tilde{R}_n}\frac{R_m^{(0)}+\tilde{R}_n}{R_m^{(0)}-\tilde{R}_n}\right)^{1/4} \times\left(1+\frac{\delta_\infty}{R_m^{(0)}}\frac{19R_m^{(0)3}+26R_m^{(0)2}\tilde{R}_n+R_m^{(0)}\tilde{R}_n^2-4\tilde{R}_n^3}{4(2R_m^{(0)}+\tilde{R}_n)(R_m^{(0)}+\tilde{R}_n)^2} +\frac{\sigma_{21}^{\infty}\chi_2}{4R_m^{(0)2}}\frac{28R_m^{(0)3}+56R_m^{(0)2}\tilde{R}_n+35R_m^{(0)}\tilde{R}_n^2+7\tilde{R}_n^3}{3(2R_m^{(0)}+\tilde{R}_n)(R_m^{(0)}+\tilde{R}_n)}\right). \tag{80}$$

Figure 9 shows the calculated $\Delta\nu_e$ and $\Delta\nu_c$ as a function of ϵ parameter for given $\tilde{R}_n$ and temperatures. The magnitude of $\Delta\nu_e$ and $\Delta\nu_c$ is important to the kinetics of heterogeneous nucleation. On one hand, we notice from Fig. 9 that

$$\Delta\nu_e\gg 1, \quad \Delta\nu_c\gg 1, \tag{81}$$

for given ϵ in the near-threshold region. This condition has been invoked in the classical theory because it allows the number of particles to be used as a continuous variable.

Downloaded 18 Apr 2007 to 129.93.16.206. Redistribution subject to AIP license or copyright, see http://jcp.aip.org/jcp/copyright.jsp

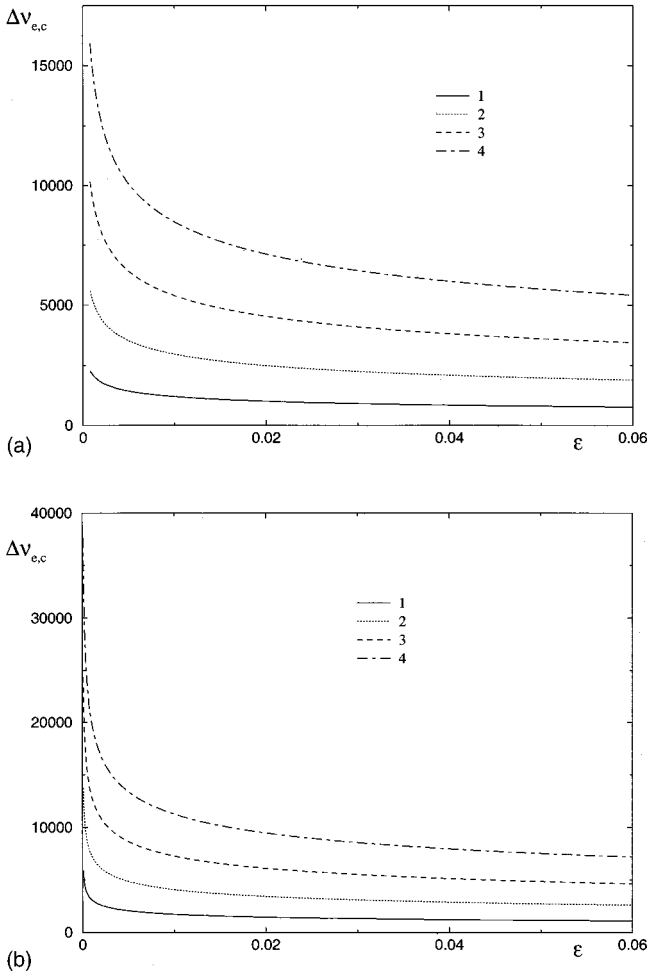

FIG. 9. Dependence of the half-width $\Delta\nu_e$ and $\Delta\nu_c$ on the ϵ parameter; curve 1: $\tilde{R}_n=5d$, curve 2: $\tilde{R}_n=10d$, curve 3: $\tilde{R}_n=15d$, and curve 4: $\tilde{R}_n=20d$. (a) $T^*=0.7$; (b) $T^*=0.9$.

On the other hand, the lower limit of ϵ parameter in the near-threshold region is controlled by the validity condition of the parabolic approximation to b,[2,4] that is, according to the classical theory

$$\frac{\Delta\nu_e}{3(\nu_m-\nu_e)}=\frac{\Delta\nu_c}{3(\nu_c-\nu_m)}\ll 1. \tag{82}$$

This condition[2] requires the height of the barrier to be higher than $2/3\sqrt{3}$, and ϵ in this model is larger than 0.005 for given $\tilde{R}_n$ and temperatures. For lower temperatures and larger $\tilde{R}_n$, this condition becomes weaker. Thus, the near-threshold region is described by values of the ϵ parameter ranging from 0.005 to about 0.06–0.08, which also describes the range of the supersaturation of the vapor. In this region one can use Eq. (79) to evaluate the barrier height, which ranges from about $3k_BT$ to a few tens of k_BT. For other values of ϵ only numerical results presented in Fig. 8 are accurate.

VI. CONCLUSION

We have developed a hybrid thermodynamic/DFT approach to the problem of heterogeneous nucleation on mesoscopic wettable particles. The thermodynamic part is similar to a classical nucleation theory.[2,4,5] The main advance over the classical approach is that the hybrid approach takes into account the first-order curvature and compressibility corrections. Such corrections cannot be given in the classical theory because parameters such as the compressibility and the Tolman length cannot be known without employing certain models for the microscopic structure of the liquid. The use of DFT allows us to find these important characteristics of the fluid, which are neglected or treated with empirical parameters in the classical theory.

Our results (Fig. 2) show that the disjoining pressure $\Pi(h)$ of the LJ liquid film near the solid surface is a monotonic function of the film's thickness h. We have confirmed several approximations to $\Pi(h)$ used in the classical nucleation theory.[2] These include the power-law approximation for thick films and the exponential approximation for thin films. Several key constants involved in these approximations, such as the Hamaker constant and the correlation length in the exponential approximation, have been evaluated directly from the DFT. In the classical theory, however, those constants were not known. That theory could only estimate them based on either experiments or other microscopic theories.

In this study we consider heterogeneous nucleation on mesoscopic wettable particles. Because of the mesoscopic size, only the first-order corrections due to the curvature (the Tolman length) and compressibility have been taken into account. Again, these corrections can be obtained in the framework of DFT but not from the classical approach. The classical approach becomes more valid when the solid particle is beyond mesoscopic, for which those first-order corrections can be neglected entirely.

We have investigated the temperature dependencies of the surface tension and the Tolman length of the liquid–vapor interface by using a nonlocal WDA-DFT. To our knowledge, this is the first study of the Tolman length using WDA-DFT. We find the WDA gives qualitatively similar results of surface tension and the Tolman length as LDA. In particular, the WDA-DFT predicts a negative sign of δ_∞, as does the LDA-DFT. This result is useful not only for this study, but also for other problems involving surfaces of large droplets.

Another main result of this work is the dependence of the chemical potential of liquid condensate on the size of the droplet $b(R)$ or the number of molecules $b(\nu)$. We find that the chemical potential is a nonmonotonic function of R or ν. A maximum appears on the $b(R)$ or $b(\nu)$ curve, which gives rise to a threshold value of the chemical potential b_{th} at R_m or ν_m. When the chemical potential of the vapor $b_1>b_{th}$, the nucleation process becomes barrierless. We also find that for large solid particles, R_m is always in the region of thick films for which the power-law approximation to Π is applicable. This fact was not obvious in the classical theory because of the lack of exact calculation of R_m. The power-law approximation has been used to obtain analytical expressions for some nucleation characteristics. Wherever the power-law approximation is applicable, e.g., for nonpolar fluids on large wettable solid particle, we find that our analytical expressions can be reduced to the classical ones[2] by neglecting curvature and compressibility corrections. Even with the ne-

Downloaded 18 Apr 2007 to 129.93.16.206. Redistribution subject to AIP license or copyright, see http://jcp.aip.org/jcp/copyright.jsp

glect, all the unknown quantities appearing in those equations become well defined in the hybrid approach. For polar fluids, however, the exponential approximation is required due to the long correlation length involved. The exponential approximation to Π is also needed for fluids on small solid particles. For the latter, the logarithmic behavior of the chemical potential due to the adsorption on the particle also becomes important. For this particle-size range our approach, which uses expansion over the small curvature of droplet, is no longer valid.

Finally, we have obtained several quantities key to the study of the kinetics of heterogeneous nucleation. These include the barrier height to nucleation, ΔW (see Fig. 8) and the half-width $\Delta\nu_e$ about ν_e, and $\Delta\nu_c$ about ν_c on the $W(\nu)$ curve. Note that a kinetic theory of heterogeneous nucleation on mesoscopic particles has been developed by other workers.[2,4] Inputs to that theory include the data shown in Figs. 8 and 9 at various nucleation conditions. Moreover, it requires the equilibrium distribution[2] of the droplet per unit volume

$$n^{(e)}(\nu)=\frac{n_n}{\pi^{1/2}\Delta\nu_e}\exp(-\Delta W)\exp\left[\left(\frac{\nu-\nu_c}{\Delta\nu_c}\right)^2\right],\quad |\nu-\nu_c|\leqslant\Delta\nu_c, \tag{83}$$

where n_n is the number of solid particles per unit volume, as well as the steady-state distribution in the near-threshold region

$$n^{(s)}(\nu)=\frac{n_n\exp(-\Delta W)}{\pi^{1/2}\Delta\nu_e\Delta\nu_c}\exp\left[\left(\frac{\nu-\nu_c}{\Delta\nu_c}\right)^2\right]\times\int_{\nu}^{\infty}d\nu'\exp\left[-\left(\frac{\nu'-\nu_c}{\Delta\nu_c}\right)^2\right]. \tag{84}$$

The steady-state rate of nucleation is given by

$$j^{(s)}=\frac{n_n w_0}{\pi\Delta\nu_e\Delta\nu_c}\exp(-\Delta W), \tag{85}$$

where w_0 is the number of molecules attached to the surface of the droplet (with size R_m) per unit time at the so-called free-molecule regime.[4] Our calculation of R_m, ν_m, ν_e, ν_c, and that shown in Figs. 8 and 9 all can be used in these formulas to investigate the kinetics of heterogeneous nucleation on mesoscopic solid particles.

ACKNOWLEDGMENTS

The authors are grateful to Professor Alexander Shchekin and Dmitriy Tatianenko for useful discussions and comments. This work is supported by the National Science Foundation.

APPENDIX A: EVALUATION OF SURFACE TENSION AND THE TOLMAN LENGTH USING WDA-DFT

The surface tension and the Tolman length can be evaluated from either molecular simulations[31–33] or the DFT.[26,28,34–36] For small R, both DFT and molecular simulations predict a positive sign of the Tolman length $\delta(R)$. However, the sign of δ_∞ (for $R\to\infty$) is still controversial due to the lack of experimental measurements. One molecular dynamics simulation[33] predicted that the Tolman length is negative, whereas another[32] predicted that it is positive. Thus far, all DFT has suggested that δ_∞ is a small negative quantity. The question is to what extent the underlying approximations in DFT, such as the random-phase approximation (RPA) or the local density approximation (LDA), affect the predicted outcome. Could the negative sign of δ_∞ be an artifact of some approximations? In a previous study[37] we examined the effects of the RPA and an improved modified mean-field approximation (MMFA) in the framework of LDA-DFT. That study showed that the MMFA leads to a slight decrease of $|\delta_\infty|$ but still predicts a negative sign of δ_∞. Here, we examine effects of WDA on δ_∞. To our knowledge, this is the first calculation of δ_∞ based on the nonlocal WDA-DFT. Results will be compared with those based on LDA-DFT.

We calculate σ_{21}^{∞} and δ_∞ by using the statistical-mechanics formulas derived by Blokhuis and Bedeaux,[34,38] which are applicable to systems with pairwise intermolecular potential. A key input for these formulas is the density profile of the planar liquid–vapor interface $\rho(z)$. It turns out that δ_∞ is strongly dependent on the symmetry of the density profile. For example, if one uses the symmetric hyperbolic-tangent density profile resulting from the gradient-expansion DFT,[39] $\delta_\infty=0$.[35,36] It is known that WDA can lead to microscopic oscillation on $\rho(z)$ at the liquid side at low temperatures and high liquid densities (above the so-called Fisk–Widom line).[40,41] In other words, the WDA can significantly change the symmetry of the density profile. It is of interest to see how this oscillation behavior in $\rho(z)$ affects δ_∞.

We notice that the original Bolokhuis–Bedeaux formulas cannot be directly applied here due to the nonlocal nature of the WDA. Generalization of these formulas can be made by replacing the pairwise potential $w_p(r_{12})$ with the effective pairwise potential $w_p(r_{12})+\phi_{hs}\omega(r_{12},\overline{\rho}(\mathbf{r}_2))$, where

$$\phi_{hs}=\frac{2\Delta\psi'_{hs}(\overline{\rho})}{1-\overline{\rho}_1-2\overline{\rho}\overline{\rho}_2}. \tag{A1}$$

Indeed, in order to calculate the surface tension and the Tolman length, one has to find the variation of the system's free energy under different coordinate transformation,[37,38] but keep the volume of the system unchanged. As was shown in our previous work,[37] the only part of the free energy which contributes to this variation is the nonlocal part, that is, according to Eq. (15)

$$F_{\text{nonlocal}}[\rho]=\int d\mathbf{r}_2\,\rho(z_2)\Delta\psi_{hs}(\overline{\rho}(z_2))+\tfrac{1}{2}\int\int d\mathbf{r}_1\,d\mathbf{r}_2\,w_p(r_{12})\rho(z_1)\rho(z_2). \tag{A2}$$

The variation is given by

Downloaded 18 Apr 2007 to 129.93.16.206. Redistribution subject to AIP license or copyright, see http://jcp.aip.org/jcp/copyright.jsp

$$\delta F_{\text{nonlocal}}[\rho]=\int d\mathbf{r}_2\,\rho(z_2)\Delta\psi'_{hs}(\overline{\rho}(z_2))\,\delta\overline{\rho}(z_2)+\frac{1}{2}\int\int d\mathbf{r}_1\,d\mathbf{r}_2\,\delta w_p(r_{12})\rho(z_1)\rho(z_2). \tag{A3}$$

Taking into account Eq. (16), after some mathematical work the variation becomes

$$\delta F_{\text{nonlocal}}[\rho]=\int d\mathbf{r}_1\int d\mathbf{r}_2\,\rho(z_1)\rho(z_2)\Bigg[\Delta\psi'_{hs}(\overline{\rho}(z_2))\times\frac{\partial\omega(r_{12},\overline{\rho}(z_2))/\partial r_{12}}{1-\overline{\rho}_1(z_2)-2\overline{\rho}_2(z_2)\overline{\rho}(z_2)}+\frac{1}{2}\partial w_p(r_{12})/\partial r_{12}\Bigg](((\delta\mathbf{r}_2-\delta\mathbf{r}_1)\mathbf{e}_r), \tag{A4}$$

where $\mathbf{e}_r$ is the unit vector in the direction of $\mathbf{r}_{12}$. The variation becomes the same as Eq. (8) in Ref. 37 by replacing the potential $w_p(r_{12})$ there with the effective pairwise potential $w_p(r_{12})+\phi_{hs}\omega(r_{12},\overline{\rho}(\mathbf{r}_2))$. The rest of the derivation of the surface tension and the Tolman length will then follow that in Ref. 37.

Thus, the generalized formula for the surface tension is

$$\sigma_{21}^{\infty}=\frac{\pi}{2}\int dz_1\int r_{12}^2\,dr_{12}\int_{-1}^{1}ds\Bigg[\frac{\partial w_p(r_{12})}{\partial r_{12}}+\phi_{hs}(z_1+sr_{12})\frac{\partial\omega(r_{12},\overline{\rho}(z_1+sr_{12}))}{\partial r_{12}}\Bigg]r_{12}(1-3s^2)\times\rho(z_1)\rho(z_1+sr_{12}). \tag{A5}$$

This formula differs from the original one by having the second term in the square bracket, due to the nonlocal function Eq. (A1). Using the integration by parts, Eq. (A5) can be written in a similar form as in Ref. 34, that is

$$\sigma_{21}^{\infty}=\pi\int dz_1\int r_{12}^2\,dr_{12}\int_{-1}^{1}ds\Bigg[\frac{\partial\rho(z_2)}{\partial z_2}w_p(r_{12})+\frac{\partial[\phi_{hs}(\rho(z_2))\omega(r_{12},\overline{\rho}(z_2))\rho(z_2)]}{\partial z_2}\Bigg|_{z_2=z_1+sr_{12}}\Bigg]\times sr_{12}\rho(z_1). \tag{A6}$$

The generalized formula Eq. (A5) or (A6) allows us to evaluate σ_{21}^{∞} by using the density profile calculated from the WDA-DFT. Results of σ_{21}^{∞} at various temperatures are shown in Fig. 10, as well as those σ_{21}^{∞} calculated from the LDA-DFT using the original formulas.[28,34] Generally, the WDA gives a lower σ_{21}^{∞} than the LDA. The difference is bigger at low temperatures above the Fisk–Widom line, where the density profile exhibits oscillatory behavior. But, the difference is still less than 7%. Previously, we showed[37] that the difference in σ_{21}^{∞} by replacing the RPA with the MMFA amounts to 20% at the low temperatures.

The generalized statistical-mechanics formula for the Tolman length is

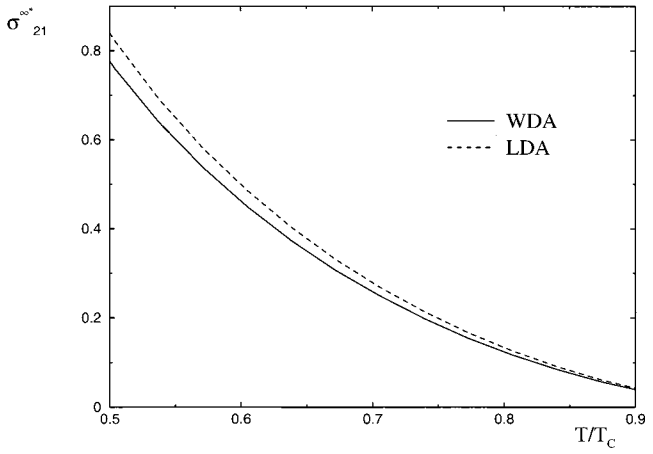

FIG. 10. Temperature dependence of the scaled surface tension $\sigma_{21}^{\infty *}=\sigma_{21}^{\infty}\pi d^2/6k_BT$.

$$\delta_{\infty}=-\frac{\pi}{4\sigma_{21}^{\infty}}\int dz_1\int r_{12}^2\,dr_{12}\int_{-1}^{1}ds\Bigg[\frac{\partial w_p(r_{12})}{\partial r_{12}}+\phi_{hs}(\rho(z_1+sr_{12}))\frac{\partial\omega(r_{12},\overline{\rho}(z_1+sr_{12}))}{\partial r_{12}}\Bigg]r_{12}(1-3s^2)\times(2z_1+sr_{12})\rho(z_1)\rho(z_1+sr_{12}). \tag{A7}$$

As in the original Blokhuis–Bedeaux formula, a condition for applying Eq. (A7) is that the density profile should be calculated using the equimolar dividing surface. Otherwise, additional terms must be included. Again, using the integration by parts, Eq. (A7) can be written in a similar way as Eq. (A6), that is,

$$\delta_{\infty}=-\frac{\pi}{2\sigma_{21}^{\infty}}\int dz_1\int r_{12}^2\,dr_{12}\int_{-1}^{1}ds\Bigg[\frac{\partial\rho(z_2)}{\partial z_2}w_p(r_{12})+\frac{\partial[\phi_{hs}(\rho(z_2))\omega(r_{12},\overline{\rho}(z_2))\rho(z_2)]}{\partial z_2}\Bigg|_{z_2=z_1+sr_{12}}\Bigg]sr_{12}\times(2z_1+sr_{12})\rho(z_1). \tag{A8}$$

The calculated δ_{∞} at various temperatures is shown in Fig. 11, along with that from the LDA-DFT. Interestingly, we find that the sign of δ_{∞} predicted by using WDA-DFT is still negative, that is, the nonlocal DFT does not qualitatively change the sign of δ_{∞}. This conclusion is an important by-product of this work.

APPENDIX B: CALCULATION OF THE CONSTANT $c(\tilde{R}_n)$

We follow the method introduced in Ref. 5 to derive $c(\tilde{R}_n)$ by using a patching condition $db(\nu)/d\nu|_{\Gamma_{31}=\Gamma_{32}}=db(\nu)/d\nu|_{R=R_n}$. First, we have from Eq. (41) that

$$\lim_{R\to R_n}\frac{db(\nu)}{d\nu}=\frac{1}{4\pi R_n^2\rho_{2\infty}(1+\rho_{2\infty}\chi_2k_BTb(\nu))}\frac{db(R)}{dR}\Bigg|_{R=R_n}. \tag{B1}$$

Next, using the patching condition and Eq. (B1), we have

Downloaded 18 Apr 2007 to 129.93.16.206. Redistribution subject to AIP license or copyright, see http://jcp.aip.org/jcp/copyright.jsp

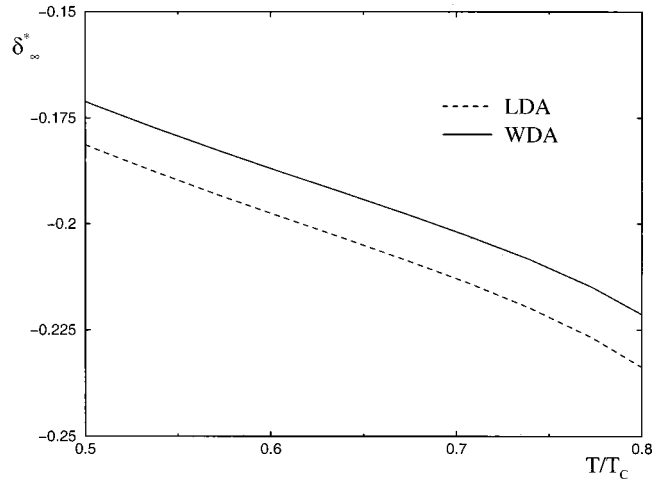

FIG. 11. Temperature dependence of the scaled Tolman length $\delta^*_\infty = \delta_\infty / d$.

$$\left.\frac{db(\nu)}{d\Gamma_{31}}\right|_{\Gamma_{31}=\Gamma_{32}} = \frac{1}{\rho_{2\infty}(1+\rho_{2\infty}\chi_2 k_B T b(\nu))} \left.\frac{db(R)}{dR}\right|_{R=R_n}. \tag{B2}$$

Finally, substituting Eq. (52) to the left-hand side of (B2) and Eq. (39) to the right-hand side of (B2), and keeping only the first-order terms of curvature and compressibility gives a linear equation for $c(\tilde{R}_n)$, that is

$$\begin{aligned} c(\tilde{R}_n) \left.\frac{dg}{d\Gamma_{31}}\right|_{\Gamma_{31}=\Gamma_{32}} & \frac{1}{\exp(b(\nu)|_{R=R_n}) - 2\Gamma_{32}/(R_n\rho_{1\infty})} \\ = \frac{1}{\rho_{2\infty}k_B T}\Bigg[& -\frac{2\sigma^\infty_{21}}{R_n^2} - \left.\frac{\partial \Pi}{\partial z}\right|_{z=z_0} + \frac{4\sigma^\infty_{21}}{R_n}\left(\frac{\delta_\infty}{R_n^2} + \frac{2\sigma^\infty_{21}\chi_2}{R_n^2}\right. \\ & \left. - \frac{\Pi\chi_2}{R_n} + \left.\frac{\partial \Pi}{\partial z}\right|_{z=z_0}\chi_2\right) - 2\chi_2 \frac{\partial \Pi}{\partial z}\Pi|_{z=z_0}\Bigg]. \end{aligned} \tag{B3}$$

Note that in classical nucleation theory[5] the crossover between the adsorbed and thin-film region was patched by using the logarithmic (adsorptive) and exponential (structural) approximations for the chemical potential and disjoining pressure, respectively.

APPENDIX C: CALCULATION OF THE DERIVATIVES FOR THE CHEMICAL POTENTIAL

To determine $d^2b(\nu)/d\nu^2|_{\nu_m}$ we first calculate $D(R) = d\nu/dR$ using Eq. (41). For $R > R_n$, the derivative is given by

$$D(R) = 4\pi R^2 \rho_{2\infty}\Bigg[1 + \chi_2 k_B T \rho_{2\infty} \times \left(b(R) + \frac{1}{3}\frac{R^3 - R_n^3}{R^2}\frac{db(R)}{dR}\right)\Bigg]. \tag{C1}$$

Since $[db(R)]/dR|_{R_m} = 0$, the second derivative

$$\begin{aligned} d^2b(\nu)/d\nu^2|_{\nu_m} &= -[1/D(R)^3][dD(R)/dR] \\ &\quad \times [db(R)/dR]|_{R_m} + [1/D(R)^2] \\ &\quad \times [d^2b(R)/dR^2]|_{R_m} \\ &= [1/D(R)^2[d^2b(R)/(dR^2)]|_{R_m}. \end{aligned}$$

With Eqs. (29), (39), (60), (61), (64), and (67), we obtain

$$\begin{aligned} \left.\frac{d^2b(\nu)}{d\nu^2}\right|_{\nu_m} &= \frac{1}{D(R)^2}\left.\frac{d^2b(R)}{dR^2}\right|_{R_m} \\ &= \frac{\sigma^\infty_{21}}{4\pi^2\rho^3_{2\infty}k_B T R_m^{(0)7}}\Bigg(-\frac{R_m^{(0)} + \tilde{R}_n}{R_m^{(0)} - \tilde{R}_n} \\ &\quad + \frac{2\delta_\infty}{R_m^{(0)}}\frac{4R_m^{(0)2} + 3R_m^{(0)}\tilde{R}_n - 2\tilde{R}_n^2}{(R_m^{(0)} + \tilde{R}_n)(R_m^{(0)} - \tilde{R}_n)} \\ &\quad + \frac{2\sigma^\infty_{21}\chi_2}{R_m^{(0)2}}\frac{2R_m^{(0)2} + 3R_m^{(0)}\tilde{R}_n + \tilde{R}_n^2}{R_m^{(0)} - \tilde{R}_n}\Bigg). \end{aligned} \tag{C2}$$

The third derivative can be expressed as

$$\begin{aligned} [d^3b(\nu)/d\nu^3]|_{\nu_m} &= -[3/D(R)^4][dD(R)/dR][d^2b(R)/dR^2]|_{R_m} \\ &\quad + [1/D(R)^3][d^3b(R)/dR^3]|_{R_m}, \end{aligned}$$

where we also used $[db(R)/dR]_{R_m} = 0$. Using Eqs. (29), (39), (60), (61), and (67), we obtain

$$\begin{aligned} \left.\frac{d^3b(\nu)^{(0)}}{d\nu^3}\right|_{\nu_m} &= \frac{1}{(4\pi R_m^{(0)2}\rho_{2\infty})^3}\frac{1}{\rho_{2\infty}k_B T}\frac{4\sigma^\infty_{21}}{R_m^{(0)4}} \\ &\quad \times \frac{13R_m^{(0)2} + 6R_m^{(0)}\tilde{R}_n - 9\tilde{R}_n^2}{(R_m^{(0)} - \tilde{R}_n)^2}, \end{aligned} \tag{C3}$$

where we just include the leading order of $R_m^{(0)}$ without considering the curvature and compressibility corrections. This is sufficient to give a reasonable estimation of the ϵ parameter via Eq. (59), that is,

$$\frac{1}{3}\epsilon^{1/2}\left(\frac{2R_m^{(0)} + \tilde{R}_n}{3R_m^{(0)}}\right)^{1/2}\frac{13R_m^{(0)2} + 6R_m^{(0)}\tilde{R}_n - 9\tilde{R}_n^2}{(R_m^{(0)2} - \tilde{R}_n^2)^{1/2}(R_m^{(0)} + \tilde{R}_n)} \ll 1. \tag{C4}$$

Using the above equation with Eq. (63), we find that the validity of the parabolic approximation requires $\epsilon < 0.08$ for $5d < \tilde{R}_n < 20d$. For larger $\tilde{R}_n$, ϵ should be even smaller.

[1] M. Volmer, *Kinetic der Phasenbildung* (Steinkopff, Dresden, Leipzig, 1939).
[2] F. M. Kuni, A. K. Shchekin, A. I. Rusanov, and B. Widom, Adv. Colloid Interface Sci. **65**, 71 (1996).
[3] D. Kashchiev, *Nucleation: Basic Theory With Applications* (Butterworth-Heinemann, Oxford, 2000).
[4] F. M. Kuni, A. K. Shchekin, and A. P. Grinin, Usp. Fiz. Nauk **171**, 345 (2001).
[5] A. K. Shchekin, D. V. Tatianenko, and F. M. Kuni, in *Nucleation Theory and Applications*, edited by J. W. P. Schmelzer, G. Ropke, and V. B. Priezzhev, 320 (JINR, Dubna, 1999).
[6] P. Adams and J. R. Henderson, Mol. Phys. **73**, 1383 (1991).

Downloaded 18 Apr 2007 to 129.93.16.206. Redistribution subject to AIP license or copyright, see http://jcp.aip.org/jcp/copyright.jsp

[7] J. E. Finn and P. A. Monson, Phys. Rev. A **39**, 6402 (1989).
[8] E. Velasco and P. Tarazona, Phys. Rev. A **42**, 2454 (1990).
[9] Y. Fan and P. A. Monson, J. Chem. Phys. **99**, 6897 (1993).
[10] P. Tarazona, Phys. Rev. A **31**, 2672 (1985).
[11] P. Tarazona, U. Marini Bettolo Marconi, and R. Evans, Mol. Phys. **60**, 573 (1987).
[12] T. F. Meister and D. M. Kroll, Phys. Rev. A **31**, 4055 (1985).
[13] J. R. Henderson, P. Tarazona, F. van Swol, and E. Velasco, J. Chem. Phys. **96**, 4633 (1992).
[14] S. Dhawan, M. E. Reimel, L. E. Scriven, and H. T. Davis, J. Chem. Phys. **94**, 4479 (1991). This paper corrects a misprint in the expression of $\omega_1(r_{12})$ in Ref. 11 and also gives slightly modified coefficients for the purpose of numerical calculations.
[15] D. W. Oxtoby, Acc. Chem. Res. **31**, 91 (1998).
[16] V. Talanquer and D. W. Oxtoby, J. Chem. Phys. **104**, 1483 (1996).
[17] K. Padilla and V. Talanquer, J. Chem. Phys. **114**, 1319 (2001).
[18] T. Getta and S. Dietrich, Phys. Rev. E **57**, 655 (1998).
[19] P. J. Upton and J. O. Indekeu, Phys. Rev. B **40**, 666 (1989).
[20] T. Bieker and S. Dietrich, Physica A **252**, 85 (1998).
[21] B. V. Derjaguin, N. V. Churaev, and V. M. Muller, *Surface Forces* (Consultants Bureau, New York, 1987).
[22] N. E. Carnahan and K. E. Starling, J. Chem. Phys. **51**, 635 (1969).
[23] J. D. Weeks, D. Chandler, and H. C. Andersen, J. Chem. Phys. **54**, 5237 (1971).
[24] X. C. Zeng and D. W. Oxtoby, J. Chem. Phys. **94**, 4472 (1991).
[25] R. C. Tolman, J. Chem. Phys. **17**, 333 (1949).
[26] V. Talanquer and D. W. Oxtoby, J. Phys. Chem. **99**, 2865 (1995).
[27] T. V. Bykov and A. K. Shchekin, Colloid J. USSR **61**, 144 (1999).
[28] T. V. Bykov and A. K. Shchekin, Inorg. Mater. (Transl. of Neorg. Mater.) **35**, 641 (1999).
[29] M. D. Donohue and G. L. Aranovich, Adv. Colloid Interface Sci. **76–77**, 137 (1998).
[30] A. I. Rusanov *Phasengleichgewichte und Grenzflachenerscheinungen* (Akademie, Berlin, 1978).
[31] A. I. Rusanov and E. N. Brodskaya, J. Colloid Interface Sci. **62**, 542 (1977).
[32] M. J. Haye and C. Bruin, J. Chem. Phys. **100**, 556 (1994).
[33] M. J. P. Nijmeijer, C. Bruin, A. B. van Woerkom, and A. F. Bakker, J. Chem. Phys. **96**, 565 (1992).
[34] A. E. van Giessen, E. M. Blokhuis, and D. J. Bukman, J. Chem. Phys. **108**, 1148 (1998).
[35] T. V. Bykov and X. C. Zeng, J. Chem. Phys. **111**, 3705 (1999).
[36] T. V. Bykov and X. C. Zeng, J. Chem. Phys. **111**, 10602 (1999).
[37] T. V. Bykov and X. C. Zeng, J. Phys. Chem. B **105**, 11586 (2001).
[38] E. M. Blokhuis and D. Bedeaux, Physica A **184**, 42 (1992).
[39] E. M. Blokhuis and D. Bedeaux, Mol. Phys. **80**, 705 (1993).
[40] R. Evans, Ber. Bunsenges. Phys. Chem. **98**, 345 (1994).
[41] R. J. F. Leote de Carvalho, R. Evans, D. C. Hoyle, and J. R. Henderson, J. Phys.: Condens. Matter **6**, 9275 (1994).

Downloaded 18 Apr 2007 to 129.93.16.206. Redistribution subject to AIP license or copyright, see http://jcp.aip.org/jcp/copyright.jsp